Transplanted Haematopoietic Cells Populate The Murine CNS In The Absence Of Irradiation

by

John Manning

B.Sc. (Kinesiology), Simon Fraser University, 2009

THESIS SUBMITTED IN PARTIAL FULFILMENT
OF THE REQUIREMENTS FOR THE DEGREE OF
MASTER OF SCIENCE

In the
Department of Biomedical Physiology and Kinesiology
Faculty of Science

© John David Willis Manning 2013

SIMON FRASER UNIVERSITY

Spring 2013

All rights reserved.
However, in accordance with the *Copyright Act of Canada*, this work may be reproduced, without authorization, under the conditions for "Fair Dealing." Therefore, limited reproduction of this work for the purposes of private study, research, criticism, review and news reporting is likely to be in accordance with the law, particularly if cited appropriately.

Approval

Name: **John David Willis Manning**

Degree: **Master of Science**

Title of Thesis: ***Transplanted Haematopoietic Cells Populate The Murine CNS In The Absence Of Irradiation***

Examining Committee:

Chair: **Dr. Tom Claydon**
Assistant Professor - Biomedical Physiology and Kinesiology, SFU

Dr. Charles Krieger
Professor - Biomedical Physiology and Kinesiology, SFU
Senior Supervisor

Dr. Fabio Rossi
Professor – Medical Genetics, UBC
Supervisor

Dr. Jonathan Choy
Assistant Professor - Molecular Biology and Biochemistry, SFU
Supervisor

Dr. Jamie Scott
Professor - Molecular Biology and Biochemistry and Health Sciences, SFU
External Examiner

Date Defended/Approved: March 8th, 2013

Partial Copyright Licence

The author, whose copyright is declared on the title page of this work, has granted to Simon Fraser University the right to lend this thesis, project or extended essay to users of the Simon Fraser University Library, and to make partial or single copies only for such users or in response to a request from the library of any other university, or other educational institution, on its own behalf or for one of its users.

The author has further granted permission to Simon Fraser University to keep or make a digital copy for use in its circulating collection (currently available to the public at the "Institutional Repository" link of the SFU Library website (www.lib.sfu.ca) at http://summit/sfu.ca and, without changing the content, to translate the thesis/project or extended essays, if technically possible, to any medium or format for the purpose of preservation of the digital work.

The author has further agreed that permission for multiple copying of this work for scholarly purposes may be granted by either the author or the Dean of Graduate Studies.

It is understood that copying or publication of this work for financial gain shall not be allowed without the author's written permission.

Permission for public performance, or limited permission for private scholarly use, of any multimedia materials forming part of this work, may have been granted by the author. This information may be found on the separately catalogued multimedia material and in the signed Partial Copyright Licence.

While licensing SFU to permit the above uses, the author retains copyright in the thesis, project or extended essays, including the right to change the work for subsequent purposes, including editing and publishing the work in whole or in part, and licensing other parties, as the author may desire.

The original Partial Copyright Licence attesting to these terms, and signed by this author, may be found in the original bound copy of this work, retained in the Simon Fraser University Archive.

Simon Fraser University Library
Burnaby, British Columbia, Canada

revised Fall 2011

Ethics Statement

The author, whose name appears on the title page of this work, has obtained, for the research described in this work, either:

a. human research ethics approval from the Simon Fraser University Office of Research Ethics,

or

b. advance approval of the animal care protocol from the University Animal Care Committee of Simon Fraser University;

or has conducted the research

c. as a co-investigator, collaborator or research assistant in a research project approved in advance,

or

d. as a member of a course approved in advance for minimal risk human research, by the Office of Research Ethics.

A copy of the approval letter has been filed at the Theses Office of the University Library at the time of submission of this thesis or project.

The original application for approval and letter of approval are filed with the relevant offices. Inquiries may be directed to those authorities.

Simon Fraser University Library
Burnaby, British Columbia, Canada

update Spring 2010

Abstract

Currently, there are no effective treatments available for patients suffering from amyotrophic lateral sclerosis (ALS), a neurodegenerative disease characterized by the progressive loss of upper and lower motor neurons. Experiments in rodents and humans with neurodegenerative diseases have shown that after bone marrow transplantation following irradiation-induced myeloablation, donor cells can be found in the central nervous system (CNS). Previous work indicates that irradiation itself may be essential for bone marrow-derived cell (BMDC) entry into the CNS. Here we attempted to determine whether myelosuppressive regimens other than irradiation will potentiate BMDC accumulation in the CNS. Transgenic mice over-expressing human mutant superoxide dismutase-1 (mSOD) develop motor neuron loss resembling amyotrophic lateral sclerosis (ALS). We treated control and mSOD mice with the chemotherapeutic agent, Busulfex (BU), and transplanted with GFP^+ BM. Sub-myeloablative doses of 60-100 mg/kg BU induced ≥80% blood chimerism in these animals. In addition, GFP^+ cells were observed in the spinal cords of both control and mSOD mice. Greater numbers of GFP^+ cells were detected in mSOD spinal cords at disease end-stage compared to controls. Histological analysis of BMDCs revealed that a large fraction of donor cells acquired the stellate morphology and immunophenotype characteristic of parenchymal microglia. These data demonstrate that BU alone can be used to achieve high level BM chimerism in mice and lead to accumulation of BMDCs in the spinal cord. These protocols could be adapted for use in humans with neurodegenerative diseases such as ALS.

Keywords: Amyotrophic Lateral Sclerosis, Bone Marrow Transplant, mSOD mouse, Lumbar Spinal Cord, Busulfan,

Dedication

For Erin and my family.

Acknowledgements

I acknowledge the advice, assistance and support I received from the following colleagues: Dr. Xiao-Yang Shan, Heather Mancell, Sapana Thakore and Christine Barr. I would like to thank the staff of the ARC at SFU, particularly Mary Dearden, Kim Beuttner, Marina MacLean, and Audrey Wang. Thanks also to my supervisory committee and examiners: Dr. Fabio Rossi, Dr. Jonathan Choy and Dr. Jamie Scott. To Dr. Charles Krieger and Dr. Coral-Ann Lewis, thank you so much for your continued support and patience throughout my graduate studies. I greatly appreciate the time you invested in me, and I couldn't ask for better mentors.

Table of Contents

List of Figures

List of Tables

Glossary

ALS	Amyotrophic lateral sclerosis
APC	Allophycocyanin
APC	Antigen presenting cell
BBB	Blood-brain barrier
B6	C57Bl/6
BM	Bone-marrow
BMDC	Bone-marrow derived cell
BU	Busulfan/Busulfex
CNS	Central nervous system
Cy3	Cyanine 3
EAE	Experimental autoimmune encephalitis
EDTA	Ethylenediaminetetraacetic acid
FACS	Fluorescence-activated cell sorting
fALS	Familial amyotrophic lateral sclerosis
FBS	Fetal bovine serum
FITC	Fluorescein isothiocyanate
GFP	Green fluoresecent protein
GVHD	Graft-versus-host -disease
HSC	Haematopoietic stem cell
ICAM-1	Intercellular adhesion molecule-1
IGF-1	Insulin-like growth factor-1
IP	Intraperitoneal
IV	Intravenous
JAM	Junctional adhesion molecule
LFA-1	Leukocyte functional antigen-1
MCP	Monocyte chemotactic protein-1
M-CSF	Macrophage-colony stimulating factor
MHC	Major histocompatibility complex
mSOD	Mutant superoxide dismutase-1
NGF	Neural growth factor
NGS	Normal goat serum

PBMC	Peripheral blood mononuclear cell
PBS	Phosphate buffered saline
PBST	0.3% Triton-X in PBS
PE	Phycoerythrin
PECAM-1	Platelet endothelial cell activation molecule-1
PECy7	Phycoerythrin-cyanine 7
PFA	Paraformaldehyde
PSGL-1	P-selectin glycoprotein ligand
VCAM-1	Vascular cell adhesion molecule-1
VLA-4	Very late antigen-4
VOD	Veno-occlusive disease
WBI	Whole body irradiation
WT	Wild-type

1. INTRODUCTION

1.1. Amyotrophic Lateral Sclerosis

Amyotrophic lateral sclerosis (ALS) is a late-onset progressive neurodegenerative disease that primarily affects motor neurons and other motor pathways, leading to paralysis and death within 4-6 years (Boillee *et al*., 2006a). The cause of the disease is unknown, other than in some patients with familial disease. Approximately 2% of ALS cases are associated with mutations in the superoxide dismutase 1 (SOD1) gene, which induces a non-cell autonomous, gain of function toxicity (Di Giorgio *et al*., 2007). The non-cell autonomous aspect of ALS pathogenesis is based on observations that neuron-specific over-expression of mutant SOD1 (mSOD) does not lead to disease over short time periods. However, if mSOD expression also includes non-neuronal cells, neuron death can ensue (Di Giorgio *et al*., 2007). It is generally believed that as both familial (fALS) and sporadic cases of ALS (sALS) display indistinguishable pathological features, findings gleaned from animal models will provide further insight into the cause of sporadic ALS. Recent studies have also reported the presence of hexanucleotide repeat *intronic* expansions in chromosome 9 and specifically in the open reading frame 72 (C9ORF72) gene, and these repeats may be involved in up to 30% of fALS, and 4% of sALS cases (DeJesus-

Hernandez *et al*., 2011; Renton *et al*., 2011). For many years, aberrant *exonic* expansions in coding DNA have been linked to other neurological disorders, such as Huntington's disease (Snell *et al*., 1993). The discovery of a locus that potentially accounts for a large portion of ALS cases would be very important for clinical testing and developing new treatment strategies.

Several mechanisms have been proposed to explain the relatively selective destruction of motor neurons in ALS, such as excitotoxicity, oxidative damage, mitochondrial dysfunction, protein mis-folding, and defective axonal transport (Boillee *et al*., 2006a). Damage to motor neurons may also be enhanced *via* damaged non-neuronal cells, through inflammation that accelerates disease progression. This inflammation is characterized by activated microglia and infiltrating T lymphocytes in regions of spinal cord motor neuron injury (Appel *et al*., 2009). These damaged areas contain increased levels of CCL2 (also known as MCP-1), which is known to enhance both monocyte and T cell tissue-directed homing (Henkel *et al*., 2006). Indeed it has been shown that further activation of these cells using macrophage-colony stimulating factor (M-CSF), results in increased inflammatory cytokine production and an exacerbation of disease symptoms (Gowing *et al*., 2009). In light of these findings, it has been proposed that the replacement of these supporting immune cells with cells having anti-inflammatory properties (Banerjee *et al*., 2008; Chiu *et al*., 2008) or cells over-expressing neurotrophic growth factors (Gowing & Svendsen, 2011), may help to slow the progression of this devastating disease.

1.1.1. Current Animal Models

SOD1 is a ubiquitously expressed enzyme that catalyses the reduction of superoxide anions into oxygen and hydrogen peroxide. Mutations in SOD1 account for approximately 20% of all familial cases of ALS. Over 150 different mutant forms of SOD1 (mSOD) have been reported in ALS patients, with the vast majority being missense mutations spanning all coding regions of the protein (Andersen, 2006). This has led to the development of several strains of transgenic mice, which express mSOD. Although each strain of transgenic mSOD over-expressing mouse varies in its degree of expression of the human gene, as well as its disease progression rate, all transgenic mSOD mice exhibit neurodegenerative pathology similar to ALS in humans (Turner & Talbot, 2008). Of these models, the most commonly studied is that expressing G93A SOD1, which exhibits a short time to disease onset and a rapid disease course (Gurney *et al*., 1994). These mice develop signs of hind-limb weakness after 12 weeks, and paralysis and premature death by 20 weeks of age.

SOD1 mutations were initially thought to cause pathogenesis *via* a loss of function, until work by Reaume *et al*. (1996) demonstrated that knocking out wild type SOD1 does not produce neurodegenerative disease. Mice lacking SOD appear healthy, however they show signs of distal neuropathy with advanced age. Similar results were obtained using cre-lox systems, in which selective reduction of mutant SOD expression leads to an extension of animal survival (Boillee *et al*., 2006b) Conversely, neurological symptoms were observed in mice

overexpressing WT SOD1, albeit after two years of age (Jaarsma *et al*., 2000). Further investigations into neuron-specific mSOD expression revealed neurodegeneration but to a lesser degree than in mice that ubiquitously express mutant SOD1 (Jaarsma *et al*., 2008). It was also found that the degenerative process is enhanced through additional mSOD expression in other CNS resident cells such as astrocytes and microglia (Di Giorgio *et al*., 2007), or ameliorated by transplanting WT SOD1 bone marrow into mSOD mice lacking endogenous microglial cells (Beers *et al*., 2006). Together, these results highlight the non-cell autonomous nature of the disease, and emphasize the role of glial cells in the degenerative process.

1.2. Microglia

Microglia are the only myeloid-derived cells that normally reside within the CNS parenchyma (Prinz *et al*., 2011). At rest, they have a branched phenotype, and through protruding processes, constantly monitor their surroundings. They are part of the body's innate immune system, and as such, perform several important functions including pathogen defence, clearance of cellular debris, and antigen presentation (Napoli & Neumann, 2009). An increase in the number and reactivity of parenchymal microglia has become a hallmark of almost all CNS pathologies (Gonzales-Scarano & Baltuch, 1999), however the regulation of these cells is poorly understood. Innate immune dysfunction is a feature of ALS, and microglial inflammatory processes contribute to disease progression and

motor neuron loss in both mSOD transgenic mice and in ALS patients (Boillee *et al*., 2006a). There is a considerable body of evidence supporting the proliferation and activation of microglia throughout ALS pathogenesis (Moisse & Strong, 2006). Positron emission tomography has provided confirmation of the gradual increase in these cells throughout the disease course (Turner *et al*., 2004). It has also been observed that microglia that express mutant SOD are more readily activated and capable of inducing more extensive neuronal death than WT microglia (Beers *et al*., 2006).

Recent findings support the notion that microglia have multiple, distinct phenotypic states, similar to those described for T lymphocytes and other tissue macrophage populations (Henkel *et al*., 2009). M1-like 'classically activated' microglia are cytotoxic and secrete ROS and inflammatory cytokines such as TNF-α and IL-12, while M2-like, or 'alternatively activated' microglia, produce high concentrations of anti-inflammatory cytokines and neurotrophic factors (Gordon & Martinez, 2010). These M2-like microglia have, at present, been further divided into 3 different functional states based on their observed genetic profiles. M2a microglia are induced by IL-4 and IL-13 secreted by $CD4^+$ Th2 cells, and can be characterized by increased arginase, FIZZ1 and YM1 expression. M2b microglia can be induced by binding immune complexes and through TLR stimulation, while the M2c or 'immunosuppressive' phenotype, is produced by TGF-β and IL-10; cytokines associated with Treg cells (Michelucci *et al*., 2009).

The origin and proliferative capacity of microglia is controversial. There is little doubt that they are of haematopoietic origin, but some experiments would also suggest that they are capable of extensive peripheral renewal (Simard & Rivest, 2004). Mice lacking the transcription factor PU.1 are deficient in microglia, and can be rescued at birth through the injection of WT bone marrow (Beers *et al*., 2006). However, there is also considerable evidence supporting the notion that minimal cellular traffic occurs between the CNS parenchyma and the periphery under physiological conditions (Vallieres & Sawchenko 2003; Chinnery *et al*., 2010). These studies claim that microglial renewal throughout life occurs through resident cell expansion and not through the contribution of peripheral progenitors. *In vivo* lineage tracing experiments by Ginhoux *et al*., (2010) reported that circulating haematopoietic progenitor cells do not contribute to homeostatic levels of microglia in the CNS. Rather, these cells originate from primitive myeloid-lineage progenitors in the yolk sac during day 8 and 9 of embryonic development. A limitation of this work is that only approximately one third of yolk sac progenitors exhibited successful genetic labelling, significantly less penetrance than is usual in these systems. More recent work has supported these claims by utilizing parabiosis and an experimental autoimmune encephalitis (EAE) model. These experiments showed that monocytes and T cells do enter the CNS, but vanish after resolution of CNS inflammation, and thus do not contribute to the static microglial pool (Ajami *et al*., 2011).

1.3. T Lymphocytes

T lymphocytes are capable of recognizing a vast array of peptide antigens, owing to the incredible variation in the T cell receptor (TCR) imparted by V(D)J junctional diversity, somatic hypermutation and a large number of α and β chain genes. The active signalling interface between T cells and antigen presenting cells (APCs), such as macrophages, is termed the immunological synapse, and collectively involves the TCR, specific peptide, major histocompatibility complex (MHC), secondary co-stimulatory molecules, and other cell adhesion molecules. This interaction allows for the maturation and clonal proliferation of the naive T cell into a particular effector subtype, depending on the cytokines present in the local milieu (Lewis *et al*., 2012). Activated $CD4^+$ T cells can become a variety of helper cells; Th1 cells, which secrete predominately inflammatory cytokines such as IFN-γ and IL-12, or Th2 cells which produce IL-4, IL-5 and IL-21 and induce B cell proliferation and maturation into antibody secreting cells. More recently described are Th17 cells, which play a major role in autoimmunity through production of IL-17 and other pro-inflammatory cytokines, and also T regulatory cells that function to keep auto-reactive cells in check and dampen the immune response through the secretion of TGF-β and IL-10 (Locksley, 2009).

The CNS parenchyma is protected from the fluctuating milieu of the blood circulation by the blood-brain barrier (BBB) and other related barrier structures such as the blood-CSF barrier. These structures are composed of specialized endothelial cells that restrict the transmigration of most peripheral blood

mononuclear cells (PBMCs) (Engelhardt & Coisne, 2011). Additionally, ubiquitously high levels of Fas ligand (Choi & Benveniste, 2004), and an inherent lack of MHC I and immune-stimulatory molecules (Galea *et al*., 2007), also render the CNS inhospitable to infiltrating cells. However, many studies have addressed the ability of T cells to penetrate the CNS of ALS patients using immunohistochemical analysis of post-mortem tissue (Troost *et al*., 1990; Kawamata *et al*., 1992). Indeed, activated T lymphocytes are capable of penetrating the healthy BBB and patrolling the CNS (Becher *et al*., 2006). Most of the infiltrating lymphocytes reported in human ALS tissue are cytotoxic $CD8^+$ cells that display TCRs suggesting oligoclonal expansion. These cells seem localize predominately in the pre-central gyri, corticospinal tracts, and anterior horns of the spinal cord (Holmoy, 2007). At post-mortem, $CD4^+$ cells are observed, albeit in lower numbers that generally lie in proximity to damaged white matter tracts, as opposed to the predominantly grey-matter associated $CD8^+$ cells (Engelhardt, 1993). While T cells may play a limited or no role in disease initiation in familial ALS models, T cell infiltration of the CNS shows a strong correlation with the rate of disease progression. In mSOD mice, predominantly $CD4^+$ T cell infiltration is observed beginning at 10 weeks of age and becomes most prominent at 14 weeks, a time point associated with disease stability. This stabilization phase appears to be associated with the induction of M2-like microglia and an increase in IGF-1 secretion (Chiu *et al*., 2008). However, as the disease progresses there is a large increase in the number of $CD8^+$ T cells, which may attenuate the survival phase, and result in extensive

motor neuron death. These $CD8^+$ cells could potentially target neurons bearing up-regulated MHC I, and kill them through the release of cytotoxic granules and/or through Fas-ligand interactions (Melzer *et al*., 2009). Although $CD8^+$ cells seem to respond to a specific antigen, as evidenced by their oligoclonally expanded TCRs, no specific endogenous neuronal peptide capable of inducing a cytotoxic lymphocyte (CTL) response has been found in ALS (Holmoy, 2007).

In order to home to and enter the CNS, T lymphocytes must first be locally activated in the secondary lymphatic tissues draining the cerebrospinal fluid (such as the cervical lymph nodes) by professional APCs (Seder and Ahmed, 2003). A plausible scenario of events likely involves initial $CD4^+$ T cell mediated activity, as this subset makes up more than 80% of cerebrospinal fluid (CSF) mononuclear cells under physiological conditions (Ransohoff *et al*., 2003). Cells of the $CD4^+$ subset recognize their specific antigens as presented on macrophages in the perivascular and subarachnoid spaces; this induces their re-activation and extravasation into the CNS parenchyma (Becher *et al*., 2006). In the parenchyma, activated M1-like microglia expressing MHC II-dependent antigen, could induce the differentiation and/or re-activation of Th1 and Th17 cells, through a local inflammatory microenvironment. Both neurons and astrocytes are capable of transforming effector $CD4^+$ cells into Tregs *in vivo*, as a means of maintaining CNS immune privilege (Liu *et al*., 2006; Trajkovic *et al*., 2004). Therefore the pro-inflammatory state of these cells is likely initially held in check by existing or induced Treg and/or Th2 cells patrolling the CNS, until the

inflammatory response has developed enough to produce a predominance of activated M1-like microglia (Mott *et al*., 2004). This neuroinflammation activates BBB endothelial cells to up-regulate MHC I, cell adhesion molecules, and chemokines, which promote further lymphocytic and monocytic traffic across the BBB (Engelhardt *et al*., 2008). If enough damage is induced, $CD4^+$ T cells become capable of 'licensing' microglial and perivascular macrophages to cross-present exogenous antigen on MHC I, allowing activation of $CD8^+$ cells in the cervical lymph nodes, leading to their homing and entry into the CNS (Calzascia *et al*., 2005). MHC I displayed peptide on endothelial cells, as well as continued stimulation by licensed APCs, are required for $CD8^+$ cells to maintain their migration and cell-specific killing capabilities in the tonically immune-inhibitory environment of the CNS (Mrass *et al*., 2006). However, no specific neuronal or myelin-associated antigen has been identified for ALS. Therefore although it is possible that $CD8^+$ cells may directly attack neurons, it is more likely that they exert their effects through bystander-mediated damage (*i.e. via* cytokines) while targeting other glial cells. Intravital microscopy has provided evidence that antigen-specific T cells may make antigen-independent contact with neurons, as well as induce indirect damage (Nitsch *et al*., 2004). Indeed, a single antigen-dependent $CD8^+$ T cell, exclusive to an oligodendrocyte-expressed peptide, was observed to kill up to 10 neurons through non-specific perforin and granzyme spill over (Göbel *et al*., 2010). This suggests that bystander-mediated neuronal damage could be a mechanism of neuronal death in ALS and other neurodegenerative diseases. Recent findings have also implicated Th17 cells in

forming these non-TCR/MHC I-specific contacts with neurons (which do not express MHC II), since they readily induce neuron death *in vitro*, and calcium-dependent axonal destruction *in vivo* (Siffrin *et al*., 2010).

1.4. Blood-Brain Barrier

There are numerous cellular interfaces between the blood, CSF, and CNS parenchyma. Blood–brain interfaces comprise both the BBB located at the endothelium of the cerebral microvessels and the blood–CSF barrier located at the epithelium of the choroid plexuses. All microvessels of the gray and white matter structures including those of the hypothalamus display a barrier phenotype characteristic of the BBB, while the four CSF-secreting ventricles of the brain possess blood-CSF junctions with greater surface area and blood flow (Keep & Jones, 1990). In addition to these regions, the capillaries of circumventricular organs such as the area postrema or the median eminence are highly permeable, which is unusual among brain structures (Johnson & Gross, 1993). CNS microvessels acquire their barrier phenotype during cerebral vasculogenesis under the influence of the Wnt/β-catenin pathway, whereas the tight choroid plexus epithelium develops even earlier during embryogenesis under the influence of Sonic hedgehog protein (Strazielle & Ghersi-Egea, 2013).

Neuronal activity within the CNS depends upon strict homeostatic conditions, and does not tolerate the uncontrolled perturbations brought on by components of the peripheral blood compartment. As such, the CNS possesses

a selective barrier that limits cellular and large molecular traffic into the parenchyma. Indeed, it was traditionally believed that the CNS is an immunologically privileged site, as allogeneic tissue grafts were much better tolerated in the nervous system compared to their original locations (Barker & Billingham, 1977). This fact, combined with early reports that the CNS was devoid of cells that constitutively express MHC I or II, and lacked an afferent lymphatic system, firmly established the belief that this compartment was ignorant to both pathogens and infiltration by immune cells. However, this contention conflicted with the 1943 ground-breaking work of Medawar *et al*., who showed that allogeneic CNS tissue grafts in hosts that had been first immunized with donor antigen were promptly rejected (Medawar, 1943). These experiments suggested that peripheral T cells must be capable of penetrating the blood-brain barrier, at least under certain circumstances. Subsequent observations of immune-mediated CNS pathologies have further confirmed these conclusions, as neuronal-antigen-specific T cells are capable of homing to and migrating across the BBB, in the absence of CNS inflammation, and subsequently inducing disease (Sospedra & Martin 2005). Therefore, it is now thought that the CNS, while not a fully immuno-privileged site, is normally a tolerogenic site, that employs multiple, selectively controlled barriers to protect its valuable and irreplaceable neuronal cells.

The most luminally located component of the BBB are the endothelial cells, which rest on a basement membrane made of collagen IV, fibronectin,

laminin, and proteoglycans. These specialized cells, through an elaborate system of tight junctions, restrict the paracellular and transcellular passage of molecules (Abbott *et al*., 2010). These junctions are approximately 2 nm wide and are comprised of several transmembrane adhesion molecules, including cadherins, junctional adhesion molecules (JAMs), occludins and claudins that link adjacent endothelial cells (Huber *et al*., 2001). As CNS tissues are extremely metabolically demanding, BBB endothelial cells also possess highly specific, polarized transport proteins, which import the required nutrients while exporting any of the toxic metabolites produced by the CNS (Patridge 2007). These proteins belong to the ATP-binding cassette family of transmembrane transporters that also efficiently remove large-molecular weight drugs that may accumulate within the cerebrospinal fluid (Loscher & Potschka, 2005).

The endothelial basement membrane delimits the vascular aspect of the perivascular space. This membrane is richly embedded with pericytes (Krueger & Bechmann 2010), important cellular constituents of the capillaries and post-capillary venules. They cover 22–32% of CNS capillaries (Dore-Duffy, 2008) and regulate many neurovascular functions such as angiogenesis, BBB maintenance, vascular stability and blood flow regulation (Winkler *et al*., 2011).

Separating this CSF-filled sub-space from the actual CNS tissue is an inner extracellular matrix called the *glia limitans*, produced by the end-feet of astrocytes, the supporting glial cells of the parenchyma. Astrocytic end-feet cover 99% of the CNS microvasculature and are a source of critical regulatory

factors for endothelial cells such as transforming growth factor-β (TGF-β), glial-derived neurotropic factor, and the fibroblast growth factor (Takeshita & Ransohoff, 2012).

1.4.1. Monocytic Cell Entry

Paracellular diapedesis occurs when monocytes roll, arrest and extravasate between the tight junctions of endothelial cells in response to an inflammatory stimulus in the CNS. For this to occur, cytokines produced on the abluminal side of the BBB, such as IL-1 and TNF-α, up-regulate selectins on the luminal surface of endothelial cells. These adhesion molecules induce low-affinity binding to monocytes causing the monocytes to roll with gradually reducing velocities and finally stop (Ivey *et al*., 2009). Once monocyte arrest occurs, the engagement of surface integrins such as leukocyte functional antigen-1 (LFA-1) and very late antigen-4 (VLA-4) with their Ig superfamily ligands ICAM-1 (CD54) and VCAM-1 (CD106) on the luminal side of the BBB, results in adhesion. These integrin-mediated interactions between monocytes and endothelial cells result in a complex signalling cascade that ultimately leads to contractility and opening of the tight junction *via* myosin light chain kinase-dependent pathways (Haorah *et al*., 2005). Both ICAM-1 and VCAM-1 are up-regulated in response to inflammation and are thought to facilitate further monocyte recruitment (Nottet *et al*., 1996).

Instances of transcellular diapedesis have also been reported, although their contribution comprises no more than 10% of monocyte extravasation events

(Carman & Springer, 2004). This form of diapedesis involves integrins on the rolling monocyte binding endothelial ICAM-1 that is up-regulated in response to inflammatory stimuli. Adhesion molecules then become concentrated on the surface of the endothelial cell and form a trans-migratory cup that guides leukocyte podosomes through the cytosol of the endothelial cell (Carman *et al*., 2007).

1.4.2. Lymphocytic Cell Entry

Intravital microscopic studies have reported that activated endothelial cells mediate the rolling of T cells *via* binding of P-selectin to PSGL-1 on lymphocytes (Piccio *et al*., 2002). However, another report identified α4-integrin/VCAM-1 interactions as responsible for this process (Vajkoczy *et al*., 2001). It may be that lymphocyte tethering and rolling involves both pathways in a semi-redundant fashion, as the individual blockade or absence of P-selectin, PSGL-1 or α_4-β_1 integrin does not have a significant impact on the recruitment of T cells to the CNS (Engelhardt & Coisne, 2011), while the simultaneous blockade of P-selectin and α_4-integrin results in a more complete inhibition of T cell rolling (Kerfoot *et al*., 2006). Arrest of T cells has been proven with Intravital microscopy and natalizumab treatment (an anti-LFA-1 monoclonal antibody) to be mainly due to T cell LFA-1 binding to ICAM-1 and ICAM-2 (Coisne *et al*., 2009). Indeed, many histological reports have described the up-regulation of Ig-superfamily molecules on the surface of the activated endothelial cells, with clusters of T cells expressing LFA-1 and $\alpha_4\beta_1$ integrin localizing in these areas (Baron *et al*., 1993;

Sobel *et al*., 1990). Once firm adhesion has occurred, T cells then begin to polarize and crawl along the endothelium until a suitable extravasation site is found (Steiner *et al*., 2010). These sites are areas where the underlying basement membrane expresses laminin α_4, but not laminin α_5 (Wu *et al*., 2009). The overall mechanism of paracellular diapedesis for T cells is not well understood other than that it may involve PECAM-1 (Graesser *et al*., 2002) as well as JAM (Del Maschio *et al*., 1999) interactions. In either case, once the passage across the endothelial cell barrier is complete, activated macrophages in the perivascular space secrete matrix metalloproteinases that dissolve the *glial limitans* and allow migration of T lymphocytes into the CNS parenchymal space (Agrawal *et al*., 2006).

1.4.3. Chemokines

Chemokines play a crucial role in the recruitment of PBMCs during inflammatory process. However, in addition to chemotaxis, they are also involved in regulating cell adhesion, cytokine release, matrix metalloproteinase secretion, T-cell differentiation, and angiogenesis (Takeshita & Ransohoff, 2012). Chemokines and their receptors that are expressed in the CNS include CXCL12-CXCR4/CXCR7, CXCL1-CXCR2, and CX3CL1-CX3CR1. CXCL12 and CXCR4 are selectively expressed in the developing and adult brain and control the migration and survival of neural precursors as well as stimulate astrocyte proliferation (Ransohoff, 2009). CXCL1 and CXCR2 have been implicated in the migration and proliferation of oligodendrocyte progenitors (Padovani-Claudio *et*

al., 2006). CX3CL1 and CX3CR1 are both constitutively expressed in CNS and modulate inflammatory reactions in microglia (Cardona *et al*., 2006), as well as recruit NK cells during EAE and in other diseases (Huang *et al*., 2006).

1.5. Irradiative Myeloablation and Bone Marrow Transplantation

Bone marrow transplantation (BMT) is an important procedure for treating a variety of haematopoietic disorders. Recipients first undergo pre-emptive depletion of their marrow compartment haematopoietic cells, in order to open up 'niches' for the engraftment of introduced donor stem cells. While this procedure shows promise for the treatment of many serious conditions, more general use must be avoided because of the risks of graft failure (Stotler *et al*., 2010), infection (Boeckh *et al*., 2003) and graft-versus-host disease (Ferrara *et al*., 2009).

Currently there are two methods of BMT that are clinically employed. Autologous stem cell transplantation involves the reinfusion of the patient's own stem cells, previously harvested, purified and cryopreserved, to reconstitute the haematopoietic compartment after administration of high-dose irradiation or chemotherapy. The infused stem cells are obtained from the patient's bone marrow at a time when the BM contains minimal or no disease-related cells. Allogeneic transplantation entails transferring stem cells from a donor to a recipient who is genetically distinct. This differs from autologous transplantation

in that the potential exists for immune rejection of the infused stem cells by the recipient (host-versus-graft disease) and for immune attack by the donor's cells against certain target tissues in the recipient (graft-versus-host disease). Graft-versus-host-disease (GVHD) results when the donor's T cells recognize the host MHC molecules as foreign and attack them. GVHD symptoms primarily manifest in the skin, gastrointestinal system and liver and can be divided into two somewhat distinct clinical entities: acute GVHD occurring in the first 90-100 days after transplantation, and chronic GVHD developing after the third month post-transplant (Ferrara *et al*., 2009). Graft rejection or graft failure can also occur as a result of insufficient/abnormal $CD34^+$ cells, or a toxic recipient microenvironment (Stotler *et al*., 2010). These complications are infrequent but can be very serious; they usually result in infectious death. Therapeutic interventions in these cases include growth factor administration or re-infusion of additional haematopoietic cells, but often these treatment strategies are either ineffective or impractical for the patient.

A commonly used experimental model for examining BMT kinetics utilizes donor bone marrow from mice that ubiquitously express GFP, allowing easy discrimination between donor and host. Recipient animals are exposed to myeloablative whole-body irradiation and transplanted with harvested donor cells that begin to reconstitute the haematopoietic system in the long bones of the host within 72 hours (Ushiki *et al*., 2010). It was initially believed that complete myeloablation was required for adequate engraftment and chimerism, but

experiments have now shown that mixed chimerism can be obtained with sub-myeloablative levels of irradiation (Bradley *et al*., 2002). However, to achieve significant engraftment at lower dosages of irradiation, it is necessary to transplant a much larger number of competitive cells in these cases. Indeed, the degree of chimerism obtained generally depends on the amount of gamma ray exposure, as well as the dosage of haematopoietic stem cells received (Nevozhay & Opolski, 2006).

Often the effectiveness of radiotherapy is limited by the tolerance of CNS structures. Acute effects of irradiation involve drowsiness and vomiting, while sub-acute and late consequences include radiation necrosis and cognitive impairment (Belka *et al*., 2001). One consequence of lethal irradiation is that it causes changes to the BBB, and produces a generalized inflammatory response (Ramanan *et al*., 2010). Reports also indicate that at the dosages required for adequate myeloablation, irradiation induces a temporary disruption of the blood-brain barrier (Li *et al*., 2004).

Infiltration of bone marrow derived cells into the central nervous system has been observed in several neurodegenerative disease models, including ALS (Solomon *et al*., 2006; Lewis *et al*., 2009), Alzheimer's disease (Malm *et al*., 2010) and others (Priller *et al*., 2006; Djukic *et al*. 2006). Overall, this work has identified at least 4 definitive $CD45^+$ CNS cell populations; parenchymal microglia, perivascular macrophages, leptomeningeal macrophages, and T lymphocytes. In each of these experiments, a significantly greater influx of

transplanted cells was observed in diseased nervous tissue compared to controls. This suggests that donor peripheral blood mononuclear cells (PBMCs) are capable of homing to, and perhaps expanding at, regions of neurodegeneration.

As all of these models utilized irradiative pre-conditioning, experiments have been done to clarify the confounding effect irradiation may have on the trans-migration of cells into the CNS. Using a lead helmet/linear accelerator technique, Mildner *et al*. (2007) observed greatly reduced cell entry into the brains of transplanted mice, compared to unprotected irradiated mice. Similarly, diminished entry of bone marrow cells into the CNS was reported in parabiotic mice in which one parabiont was irradiated, and the other protected through whole body shielding (Ajami *et al*., 2007). These findings suggest that CNS engraftment by peripheral cells is at best a rare phenomenon, and that experimental manipulation, such as irradiation and the introduction of non-circulating progenitor cells is necessary to enhance migration into the brain and spinal cord.

1.6. Alternative Myeloablative Regimes

Treatment with the alkylating agent, busulfan (BU), in combination with high-dose cyclophosphamide (CY), is the most commonly utilized BMT pre-conditioning regime besides whole body irradiation (WBI) in humans (Litzow *et al*., 2002). In general, both regimens are associated with similar rates of long-

term, disease-free survival. Busulfan is mainly toxic to early progenitors and bone marrow cells, sparing a large portion of the mature cells of the adaptive immune system (Bacigalapu *et al*., 2000). For this reason it often paired with CY, which is both antineoplastic and immunosuppressive. Recipient immunosuppression is particularly important in allogeneic transplantation so that rejection is prevented and engraftment of the donor haematopoietic system is permitted. While BU/CY myeloablation regimes produce similar results to irradiation, both drugs are not without their complications. BU induces widespread inflammation and damage to endothelial cells in the liver, lungs, brain and kidney (Hassan *et al*., 1989a). CY causes similar destruction and is most often associated with liver toxicity when it is converted to its active form, phosphoramide mustard, through cytochrome P450 enzymatic metabolism (Hassan *et al*., 2000).

However, one advantage of these myeloablation protocols is that BU alone is capable of inducing stable chimerism, even at sub-myeloablative doses (Yeager *et al*., 1993). This benefit, along with its tendency to leave the adaptive immune system intact (Jopling & Rosendaal, 2001), provides a means of side-stepping the two major limitations of irradiative BMT pre-conditioning when performing autologous BMTs: immunosuppression and adequate chimerism. While the reported complete myeloablative dose for BU appears to be around 150 mg/kg (Jopling & Rosendaal, 2001; Hsieh *et al*., 2007), instances of high level chimerism (≥80%) have been reported with dosages as low as 50 mg/kg

(Yeager *et al*., 1993), and stable chimerism with only 20 mg/kg (Andersson *et al*., 2003; Barry, 2003 *unpublished work*).

1.6.1. Action and Pharmacokinetics of Busulfan

BU is a potent cytotoxic drug and bifunctional alkylating agent. Through the release of its methanesulfonate group BU produces carbonium ions, which alkylate the DNA of targeted cells, resulting in the formation of cross-linkages between the bases adenine-guanine and guanine-guanine (Iwamoto *et al*., 2004). This prevents the cell from replicating its DNA and then synthesizing RNA or proteins; it is therefore lethal to rapidly dividing cells. Low doses of BU selectively depress granulocytic cells, while increasing dosages produce more general myelotoxicity and bone marrow ablation through cell death (Buggia *et al*., 1994). Experiments in rodents and humans have shown that even low doses of BU can result in the prolonged depression of haematopoietic progenitor cells, by reducing their ability to differentiate into progeny (Chaney & Sancar 1996). Comparably higher doses cause significantly greater DNA and genetic damage, killing most early progenitor cells in the bone marrow. The theory behind this selective marrow cell toxicity is that undifferentiated stem cells in the G1-phase of the mitotic cycle are relatively susceptible to alkylation by BU. Once this alkylation occurs, the cell is incapable of further differentiation and progression to mitotic stages past G2 (Buggia *et al*., 1994). Microscopic evidence supports this notion, given that many stem cell populations have arrested cell division after BU treatment. But the reasons behind the seemingly higher resistance of

differentiated cells are less well understood. It has been proposed that these cells are exposed to BU primarily in the S-phase of the cell cycle, when active DNA repair may reduce the damage caused by the drug (Dunn 1974; Bishop & Wassom 1986).

It has been demonstrated that BU is rapidly cleared from the blood of mice following IV injection, with only 10% of the administered dose being present after 5 or 10 minutes (Bishop & Wassom 1986). This rapid tissue distribution likely accounts for the short half-life of the drug in the circulation. This finding was discovered through positron emission tomography in primates, by radiolabelling the alkylating portion of the molecule. Significant drug levels were observed in the liver, lungs and brain, with the liver accumulating the largest amount of BU, which was approximately 9-fold higher than brain, during a 45-minute observation period (Hassan *et al*., 1992). Reports indicate that ≤ 50% of the administered dose of BU is recovered in the urine, with ≤ 3% of that which is excreted remaining in a biologically active form (Hassan *et al*., 1989a). Most of the drug is irreversibly bound to plasma proteins such as albumin, or metabolized through conjugation with glutathione, both spontaneously and through glutathione S-transferase. (Marchand 1987, *unpublished results*).

In general, the side effects associated with BU occur around 3-4 days following acute high dosage treatment, or with chronic administration. These are generally all attributed to genetic damage produced by the drug. The relative selectivity of BU for rapidly dividing cells has been used to explain its differential

actions among organ systems (Hassan 1999). Many investigators have pointed out the pharmacodynamic relationship between high-level systemic exposure and the occurrence of hepatic veno-occlusive disease (VOD), interstitial pneumonia, cataracts, mucositis and convulsions in patients (Beelen *et al*., 1989).

As BU is primarily processed in the liver, this organ is particularly prone to damage by the drug (Hassan *et al*., 1987). VOD occurs when a hepatic lesion forms, creating obstructions of the small intra-hepatic venules and damage to the surrounding hepatocytes. It is considered to be one of the major problems related to BMT preconditioning with BU, and incidences of VOD have been reported to be as high as 20-40% in transplant patients treated with high-dose BU (Grochow *et al*., 1989; Vassal *et al*., 1990).

BU also achieves concentrations in the CSF approximately equal to those in the blood plasma (Hassan *et al*., 1989b). In humans, the drug rapidly enters the brain and about 20% of the total injected dose remains in the brain tissue (Gibbs *et al*., 1997). This property makes BU ideal for the treatment of tumorigenic cells in the CNS, but also must be considered when using it for other applications such as BMT (Kalifa *et al*., 1992). Neurological complications such as seizures and altered mental state have been reported with moderate to high dosages (Hassan *et al*., 1996), however these cases can be effectively remedied with anti-convulsive medications, such as phenytoin (Fitzsimmons *et al*., 1990).

2. JUSTIFICATION OF STUDY AND HYPOTHESES

2.1. Justification of study

The goal of this work was to develop GFP^+ chimeric mSOD mice, and observe if haematopoietic cell entry into the CNS would occur in the absence of irradiation. Previous experiments have suggested that irradiation is a necessary factor allowing significant monocytic cell entry into the CNS parenchyma (Mildner *et al*., 2007; Ajami *et al*., 2007). Given the negative side effects associated with whole body irradiation, such as immunosuppression and widespread inflammation, we set out to generate an improved model utilizing sub-myeloablative dosages of BU. Using this model, we explored rates of peripheral blood and bone marrow reconstitution with various dosages of BU, and examined the degree of cell entry into the CNS at different time periods post-transplant, in both control and mSOD GFP^+ chimeric mice.

2.2. Objectives and hypotheses

Objective 1

To determine whether stable GFP^+ chimeric mice can be created using low to moderate dosages of BU prior to whole bone marrow transplant.

Hypothesis 1

Given its semi-selective preference for destroying haematopoietic progenitor cells (Chaney & Sancar 1996), as well as reports of its ability to induce stable low-dose chimerism (Yeager *et al*., 1993), we hypothesize that BU, when used as a pre-conditioning agent before the transplantation of bone marrow from GFP^+ donors, will produce lasting peripheral blood and bone marrow chimerism.

Objective 2

To observe histologically if cell entry into the CNS occurs in chimeric animals pre-conditioned with BU; to determine the time course of BMDC entry into the CNS parenchyma; and to establish whether greater cell numbers accumulate in the CNS of mSOD mice, compared to WT animals.

Hypothesis 2

Due to its tendency to disrupt endothelial cells even at low dosages (Zeng *et al*., 2010), we hypothesize that treatment with BU will also disrupt the BBB to such a degree that transplanted GFP^+ PBMCs will enter and take up residence in the CNS.

3. EXPERIMENTAL METHODS

3.1. Animals

Two lines of mice over-expressing the G93A mutant human transgene for CuZn (SOD1) were used in this study; 6SJL- TgN(SOD1-G93A)1Gur (SJL/B6) and B6.Cg-Tg (SOD1-G93A)1Gur/J (B6). Both G93A strains over-express mSOD by approximately 25-fold compared to non-transgenic WT littermates. These mice develop symptoms of motor neuron degeneration primarily in their hind limbs, resulting in weakness and eventual paralysis. SJL/B6 mSOD mice were bred from progenitor stock obtained from Jackson Laboratories and were maintained as heterozygotes by backcrossing mSOD males with non-transgenic females. Pups were genotyped for the mSOD transgene using a PCR assay based on genomic DNA extracted from ear tissue, as established by Gurney *et al*., (1994). B6 mSOD mice were purchased from Jackson Laboratories. Age-matched, non-transgenic B6 and SJL/B6 mice were used as controls and sacrificed at the same time points as mSOD animals.

Mice that ubiquitously express GFP under the control of the B-actin promoter (C57BL/6; GFP/CD45.2) were obtained from Dr. I. Weissmann *via* Dr. Fabio Rossi (University of British Columbia, Vancouver, BC) and were bred and maintained as heterozygotes at the Simon Fraser University Animal Research

Facility (ARC). GFP-expressing mice aged 8 weeks to 6 months served as BM donors and BM was harvested by flushing femur and tibiae with sterile PBS. Female BM recipients received only female BM whereas male recipients received either male or female BM to minimize any graft-versus-host effects due to minor histocompatibility differences.

All animals were supplied with food and water *ad libitum*. Protocols governing the use of animals were approved by review committees of Simon Fraser University and the University of British Columbia, and were in compliance with guidelines published by the Canadian Council on Animal Care and international guidelines, including the NIH Guide for the Care and Use of Laboratory Animals as well as the EEC Council Directive. Institutional approvals are available upon request.

3.2. Myeloablation and Transplantation

Control and pre-symptomatic SJL/B6 mSOD mice aged 9 weeks were used for experiments 1-3, whereas experiments 4-6 utilized control and pre-symptomatic B6 mSOD mice aged 6 weeks in order to make more direct comparisons with our previous irradiative myeloablation datasets (Lewis *et al*., 2009; Solomon *et al*., 2006). BU (Busulfan for injection, Otsuka Pharmaceuticals, Japan) was diluted from a stock solution to a concentration of 3 mg/mL using sterile PBS.

Group 1: Control (n=3) and mSOD (n=1) SJL/B6 mice received 80 mg/kg BU (diluted and stored at 4°C for a number of days) delivered in 4 doses of 20 mg/kg daily *via* intraperitoneal (IP) injection for 4 days followed by intravenous (IV) tail-vein injection of 500,000 enriched GFP^+ BM cells, 24 hours after the final BU dose. This protocol is based on unpublished work by Christopher Barry carried out under the supervision of Dr. Keith Humphries (Terry Fox Laboratories, Vancouver, BC). The GFP^+ BM donors were treated with 150 mg/kg of 5-fluorouracil (5-FU, Hospira, USA), 4 days before BM harvest to increase the number of cycling HSCs. 5-FU is selectively toxic to rapidly dividing cells and induces the cycling of quiescent HSCs within the BM. (Szilvassy *et al*., 1999). 100 µL blood samples from treated mice were taken beginning at 3 weeks post-transplant and analysed *via* flow cytometry (FACS Aria, Becton-Dickenson, NJ, USA) to determine the proportion of donor-derived PBMCs.

Group 2: Control (n=13) and mSOD (n=12) SJL/B6 mice were treated with 100 mg/kg BU delivered in 5 fractionated IP doses of 20 mg/kg a day for 5 days (below the reported myeloablative dose of 150 mg/kg). 24 hours after their final BU treatment, mice received 30 million GFP^+ non-enriched BM cells *via* IV tail-vein injection and PBMC chimerism was again analysed 3 weeks post-transplant. Tissue was collected once mice had reached disease end-stage.

Group 3: Control SJL/B6 mice (n=6) were treated with daily IP injections of BU (diluted immediately before use) at a dose of 20 mg/kg for 5 days (total dose 100

mg/kg). 24 hours after the final BU treatment mice received 30 million GFP^+ BM cells. Blood samples were collected beginning at 1 week post-transplant. Mice were sacrificed at 2 (n=3) and 4 (n=3) weeks post-transplant to analyse the kinetics of GFP^+ cell entry into the spinal cord.

Group 4: Control C57Bl/6 mice were treated with 60 mg/kg (n=8) and 80 mg/kg (n=8) BU. Transplantation protocol was the same as above, although the number of GFP^+ BM cells was reduced to 15 million per animal. Blood samples were collected weekly beginning at 1 week post-transplant. Mice from each treatment group were sacrificed at 2 weeks (60 mg/kg; n=4 80 mg/kg; n=4) and 4 weeks (60 mg/kg; n=4 80 mg/kg; n=4) post-transplant to analyse the kinetics of GFP^+ cell entry into the spinal cord.

Group 5: Control B6 (n=8) and G93A mSOD (n=8) B6 mice were treated with 60 mg/kg (4 mSOD/control pairs) and 80 mg/kg (4 mSOD/control pairs) and taken to end stage. Blood was collected weekly until disease end-stage to assess PBMC chimerism. Bone marrow was additionally harvested to assess disparities between blood and marrow chimerism.

Group 6: Control (n=1) and mSOD (n=3) SJL/B6 mice were treated with 100 mg/kg BU and 200 mg/kg Procytox, (Cyclophosphamide for injection) to assess the effect of combining immunosuppression with Busulfan treatment.

3.3. Flow Cytometry

Chimerism was determined by comparing the proportion of circulating GFP^+ cells to total number of PBMCs. PBMCs from weekly blood samples were additionally labelled with lymphoid (CD3 for T cells, CD45R for B-cells; conjugated to a phycoerythrin-Cy7 fluorophore) and myeloid (Gr-1 for granulocytes, CD11b for monocytes; conjugated to allophycocyanin fluorophore) lineage markers to confirm HSC reconstitution (eBiosciences, San Diego, CA). Results were analysed using FlowJo software (Treestand, Ashland, OR)

3.4. Tissue Processing

Mice were euthanized using CO_2 and transcardially perfused with 30 mL PBS followed by 30 mL 4% paraformaldehyde (PFA). The spinal cord was dissected, post-fixed in 4% PFA overnight at 4°C, and then immersed in 20% sucrose at 4°C overnight for cryoprotection. After cryoprotection, tissue was embedded in TissueTek O.C.T. and stored at -80°C until cryosectioning in 30 µm slices as described in Solomon *et al*., (2006).

3.5. Immunohistochemistry

Free-floating spinal cord sections underwent immunohistochemical analysis as described in Lewis *et al*., (2009). To identify macrophages, polyclonal rabbit α-Iba-1 (1:1000; Wako, VA, USA) antibody was used. Blood vessel endothelium was labelled using monoclonal rat α-CD31 (1:800; PECAM1; BD

Pharmingen, San Diego, CA). Monocytes were identified using monoclonal antibodies to rat α-CD11b and α-CD68 (1:1000; Serotec, Raleigh, NC) whereas granulocytes with monoclonal rat α-Gr-1 (1:1000; BD Pharmingen, San Diego, CA). Monoclonal rat α-CD3 and α-CD8 antibodies (1:1000, 1:500; BD Pharmingen, San Diego, CA) were used to identify and classify T lymphocytes. Secondary antibodies used were either polyclonal α-rabbit Cy3-conjugated IgG (Iba1 visualization; Jackson Immunoresearch) or polyclonal α-rat Alexa568-conjugated IgG (CD3, CD8, CD11b, CD31 visualization; Molecular Probes). Immunolabeled sections were slide mounted and coverslipped using Vectashield mounting medium with DAPI.

3.6. Analysis

Spinal cord sections were analysed using a Leica epifluorescence microscope. GFP^+ cells from each mSOD and control mouse were quantified over 15 (Groups 1,2,4,5,6) or 20 (Group 3) lumbar spinal cord sections separated by at least 150 μm and were classified according to morphology as previously described in Vallieres & Sawchenko, (2003). The phenotypes of GFP^+ BMDCs were analysed using immunohistochemistry, and the numbers of $GFP^+/Iba1^+$ or $GFP^+/CD3^+/CD8^+$ BMDCs were quantified over 5 lumbar spinal cord sections from each experimental animal in groups 1-6. CD11b quantification was also done for mice from group 3. Quantitative assessment of GFP^+ cells within the

spinal cords of mSOD and control mice was statistically evaluated using SPSS software and a Student's t-test; significance was taken at $p<0.05$.

4. RESULTS

4.1. Peripheral Blood and Bone Marrow

Group 1 (n=4) treated with 80 mg/kg BU and 500,000 5-FU enriched BM cells did not exhibit successful re-engraftment as indicated by the absence of GFP^+ cells in the peripheral blood.

For **Group 2**, the BU dose was raised to 100 mg/kg to increase the level of myelosuppression, and mice were injected with 30 million, *non-enriched*, GFP^+ BM cells, as our lab has had previous success in creating chimeric mice using these cells following irradiation as the form of myeloablation (Solomon *et al*., 2006; Lewis *et al*., 2009). Using this protocol, effective BM engraftment was obtained in a portion of mice (n=4 control, n=4 mSOD), and successful transplants exhibited 75.7 ± 9.7% (mean ± standard error; averaged over mSOD and control groups) PBMC chimerism at 3 weeks post-transplant, which increased to 84.4 ± 7.3% by 5 weeks post-transplant. PBMC chimerism levels in successfully engrafted mice were relatively stable over the course of disease progression, and analysis of femoral bone marrow at end-stage indicated that 71.2 ± 7.3% of BM cells were donor derived 9 weeks post-transplant (Figure 1).

Figure 1. High-level blood chimerism was obtained in a portion of SJL/B6 control and mSOD mice treated with 100 mg/kg BU and non-enriched bone marrow

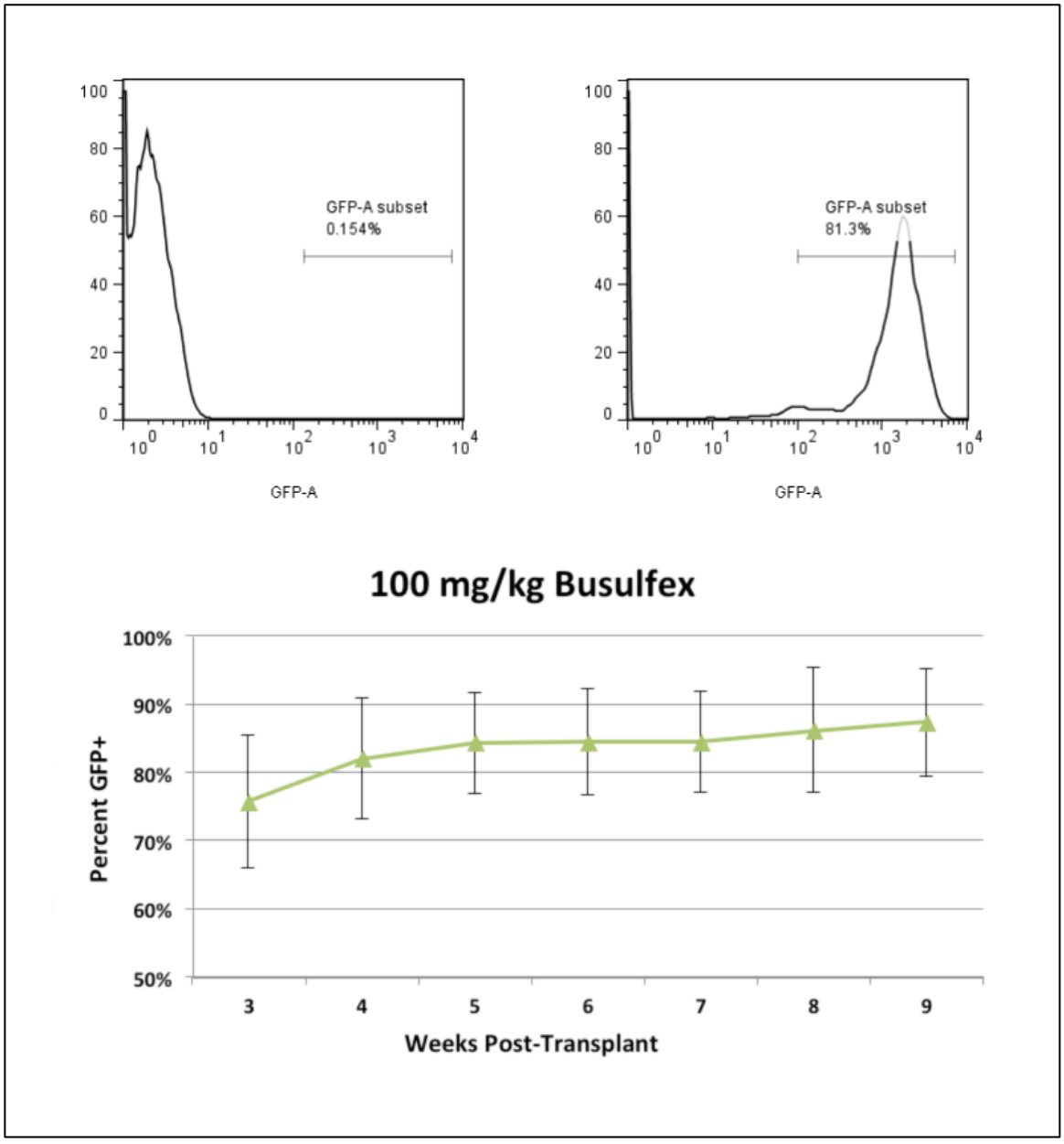

Blood samples collected from mice treated with 80 mg/kg BU and 5-FU enriched bone marrow showed no sign of GFP^+ PBMCs when examined at 3 weeks post-transplant (top left panel). However, in a portion (n=8) of mice treated with 100 mg/kg BU and non-enriched bone marrow, successful chimerism was observed (top right panel). This chimerism exceeded (≥80%) at 4 weeks post-transplant, and persisted until disease end-stage (bottom panel).

Repeated trials using this protocol yielded highly variable results with some mice exhibiting high levels of donor cell engraftment and others none at all. Intermediate levels of chimerism were never observed at 3 weeks post-transplant. Out of 25 mice treated, only 8 demonstrated successful BM engraftment of donor cells. The reason for unsuccessful BM reconstitution may have been due to technical difficulties associated with IV tail-vein injection of BM, although no obvious difficulties were encountered with BM cell preparation or injection. Incidents of unsuccessful BM engraftment after treatment with high doses of BU have been reported elsewhere (Barry, 2003*, unpublished work*). Investigation into factors that might contribute to the high number of unsuccessful transplants suggested that the stability of BU once mixed with PBS is limited (Jopling & Rosendaal, 2001).

To determine if using freshly prepared BU improved the frequency of successful BM re-engraftment, **Group 3** (n=6 control mice) was treated with freshly diluted BU rather than that which had been diluted and stored for several days at 4°C. Levels of chimerism were analysed at 1-week post-BM transplant, and rates of myeloid and lymphoid PBC reconstitution were analysed by immunolabelling PBMCs with antibodies to Gr-1 and CD11b for myeloid cells, and CD3 and CD45R for lymphoid cells. Given that in the previous trial either high levels or absent PBMC chimerism was observed in our mice, blood samples

were collected starting at 1 week post-transplant to investigate whether some mice reached transient levels of chimerism.

By using freshly prepared BU, five out of six treated mice from Group 3 exhibited successful re-engraftment as indicated by the presence of GFP^+ donor-derived PBMCs. At 1-week post-transplant, levels of GFP^+ PBMCs were highly variable and ranged from 7.9 to 52.0%. Myelomonocytic cells were rapidly reconstituted (65.5 ± 24.7% GFP^+) while lymphoid cell reconstitution (13.8 ± 7.8% GFP^+) lagged behind, likely due to the minimal immunosuppressive effect of BU, and the longer maturation time of these cells. Blood analysis at 2 weeks post-transplant indicated that in one mouse reconstitution had been unsuccessful, but in all other mice, PBMC chimerism levels had increased from the previous week. In successfully transplanted mice, near complete PBMC chimerism averaging at 97.5 ± 0.4% GFP^+ was observed 4 weeks post transplant (Figure 2). Analysis of the BM compartment at this time revealed an average of 88.4 ± 11.1% cells to be GFP^+. The results of this trial suggest that employing freshly diluted BU increases the frequency of successful BM transplantation and improves the reconstitution rates for PBMCs in excess of 95% (Table 1).

Figure 2. Kinetics of myeloid and lymphoid reconstitution in SJL/B6 control mice treated with 100 mg/kg freshly diluted Busulfan

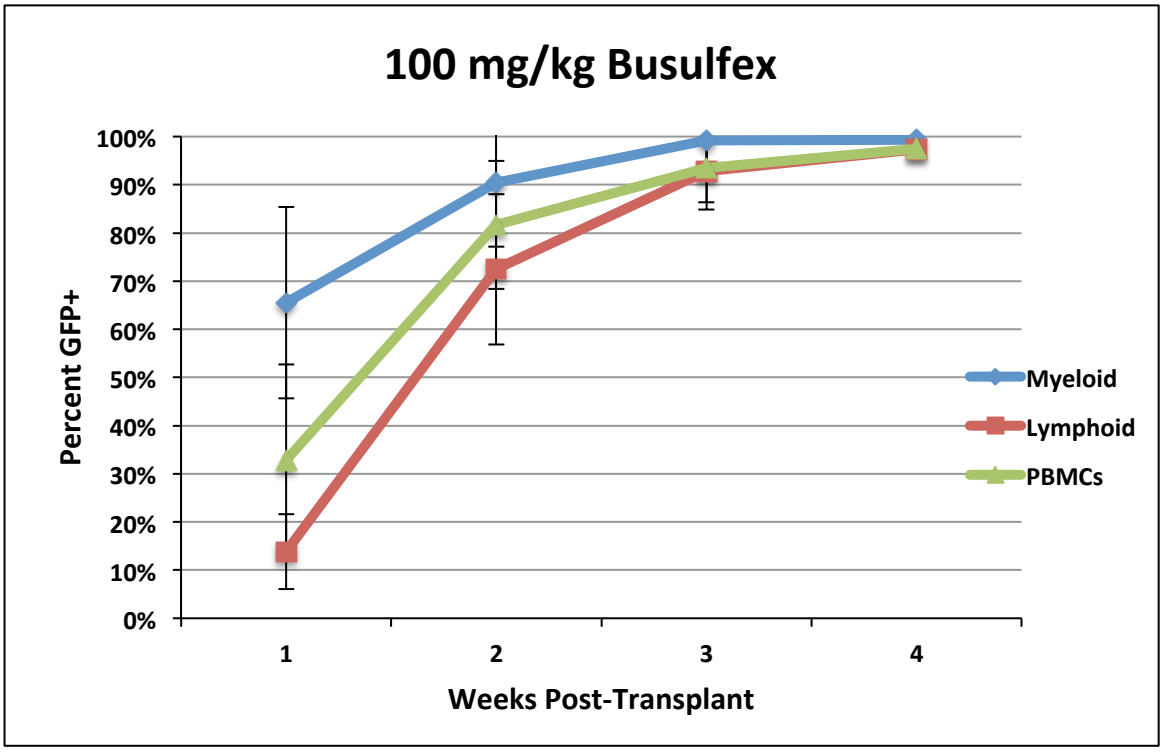

PBMC chimerism was variable at one-week post transplant. Gr-1$^+$ and CD11b$^+$ (pooled together) myeloid lineage cells (in blue) were rapidly reconstituted during this time. B220$^+$ and CD3$^+$ (pooled) Lymphoid cells (in red) took longer to reconstitute, likely due to the weak immunosuppressive nature of BU and the longer maturation time of these cells.

Table 1 – Comparing treatment efficacy in SJL/B6 mice from groups 2 and 3

	Treatment Protocol:	
	100 mg/kg BU (**Group 2**)	100 mg/kg fresh BU (**Group 3**)
Number of successfully reconstituted animals:	**8/25**	**5/6**
PBMC chimerism at 4 weeks post-transplant:	**82.0 ± 8.9%**	**97.5 ± 0.4%**

While the use of freshly prepared BU increased the effectiveness of our protocol, it was thought that a potential problem could be due to a major histocompatibility mismatch (MHC) between our B6 donors (MHC haplotype $H2^b$) and our SJL/B6 recipients (MHC haplotype $H2^b$, $H2b^{/s2}$ or $H2^{s2}$). As stated above, BU is known to myelosuppress, while sparing long-lived memory B and T lymphocytes of the adaptive immune system. In order to control this potential problem, we switched to syngeneic B6 control and G93A mSOD mice for Groups 4 and 5. B6 mSOD mice possess a longer progression time to end-stage (22-24 weeks) compared to the SLJ/B6 mSOD (18-20 to weeks), but both G93A strains over-express mutant SOD1 by approximately 25-fold compared to non-transgenic WT littermates (Alexander *et al*., 2004).

Of 16 syngeneic mice treated from **Group 4**, all exhibited apparent GFP^+ PMBC chimerism. The purpose of this group was to observe if rapid engraftment was possible with the lower pre-conditioning doses of 60 and 80 mg/kg BU. With 60 mg/kg (Figure 3a) initially there was a small percentage of GFP^+ PBMCs (4.49

± 1.41%) at week 1, however this increased to 41.33 ± 10.33% by week 2. By week 4, more than half (52.70 ± 6.22%) of PBMCs were GFP^+ in the 60 mg/kg mice. For the 80 mg/kg group (Figure 3b), early GFP^+ cell levels were much higher (25.66 ± 12.12%), presumably due to the greater suppression of host cells with the increased dose. In these mice, by 2 weeks, more than half of the PBMCs (55.31 ± 14.46%) were donor origin, and by 4 weeks chimerism of 64.35% ± 6.05% was apparent.

Myeloid cells recovered promptly, with the 60 mg/kg and 80 mg/kg groups possessing 31.34 ± 7.42% and 67.26 ± 14.60% respectively, by the end of week 1. A burst in granulocytes and monocytes was observed at week 3, possibly in response to the lingering systemic inflammation associated with BU treatment. This increased the GFP^+ myeloid cell proportions briefly to 84.51 ± 3.68% in the 60 mg/kg group and 94.78 ± 2.92% in the 80 mg/kg group. By week 4, this surge had subsided, and blood levels of GFP^+ myeloid cells had declined to 72.57 ± 10.50% and 84.22 ± 8.02%, respectively, in each group.

Lymphoid reconstitution was much slower at 60-80mg/kg BU than previously observed with 100 mg/kg BU, beginning with 3.03 ± 1.41% for 60 mg/kg and 5.69 ± 4.42% for 80 mg/kg after one week. At these early time points, GFP^+ lymphocytes are likely mature T cells from the donor BM, as T cell development in the thymus requires approximately 3 weeks (Mosley & Klein, 1992). In any case, the number of GFP^+ lymphocytes rose slowly in both groups,

and accounted for over half of all blood lymphocytes by week 4 in both the 60 mg/kg (53.05 ± 3.27%) and 80 mg/kg (66.69 ± 7.43%) groups.

Figure 3a. Kinetics of myeloid and lymphoid reconstitution in B6 control mice treated with 60 mg/kg freshly diluted Busulfan

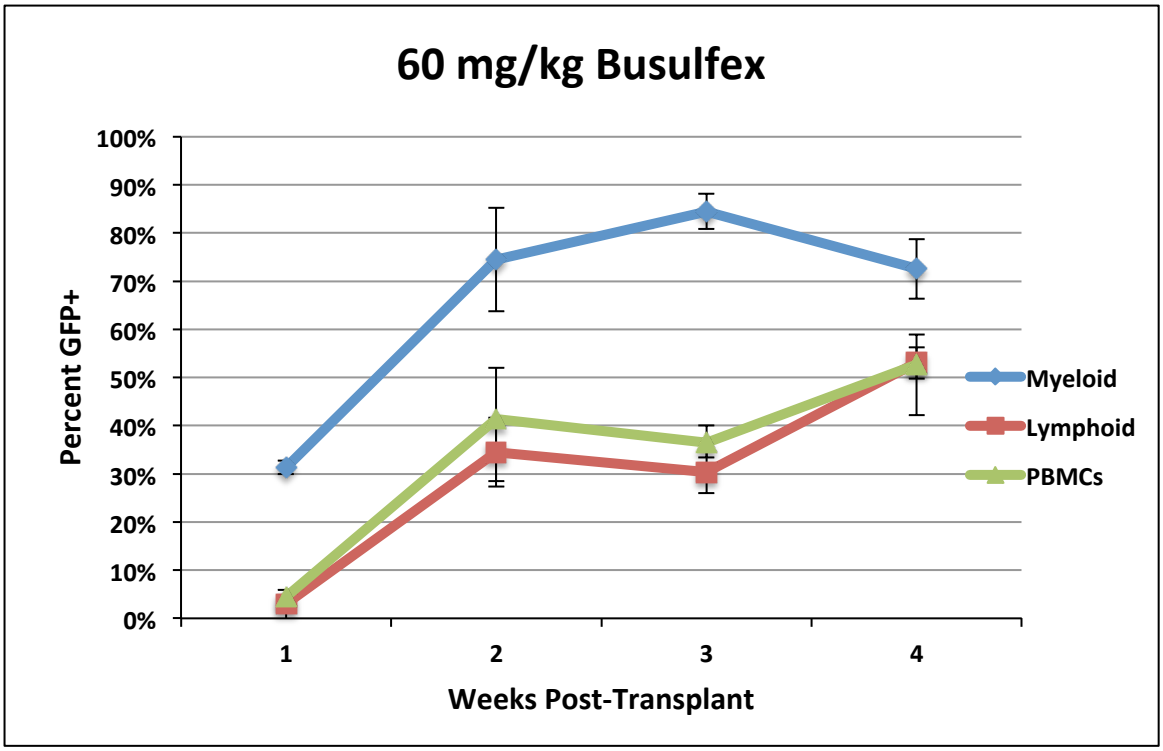

Moderate chimerism was obtained over a short time course with 60 mg/kg BU. GFP^+ cells made up over 50% of PBMCs by 4 weeks post-transplant. Quantitative data is also shown in Fig. 4c.

Figure 3b. Kinetics of myeloid and lymphoid reconstitution in B6 control mice treated with 80 mg/kg freshly diluted Busulfan

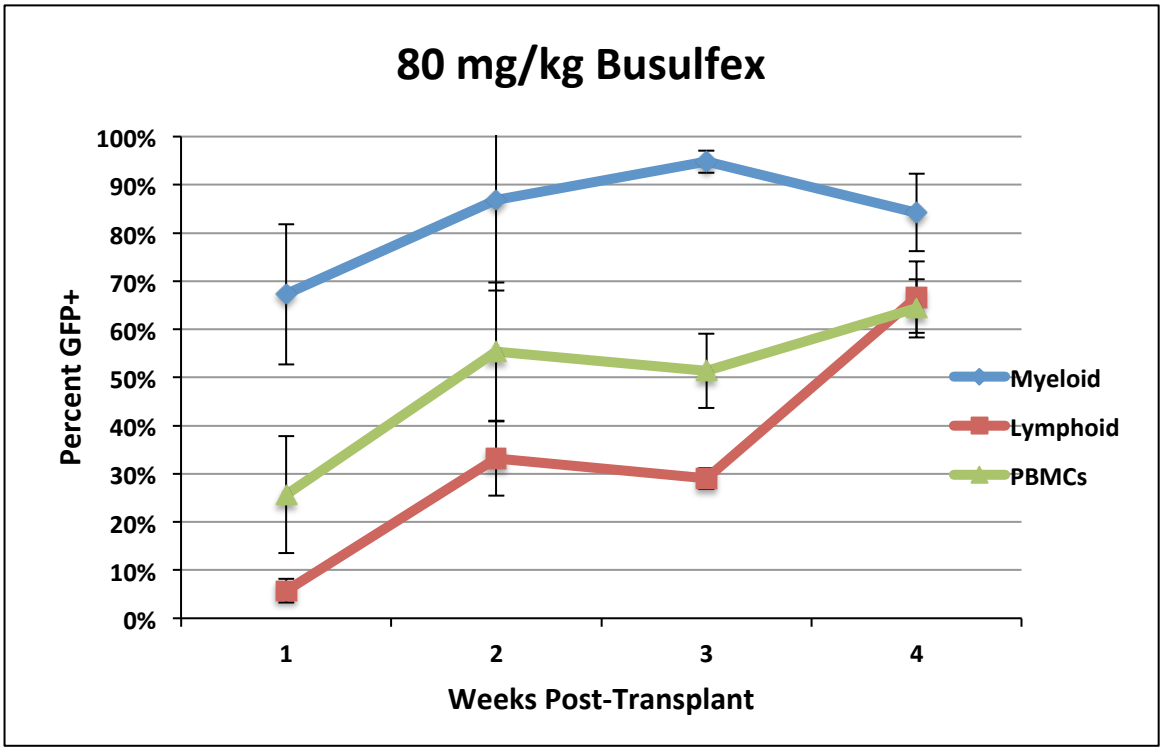

Myeloid cell reconstitution was more rapid with the 80 mg/kg dose compared to 60 mg/kg BU. However, the slower repopulation of lymphoid cells was similar for both BU doses.

As the percentage of GFP^+ cells in the peripheral blood continued to increase at 4 weeks, we decided to analyse weekly blood samples from transplanted control and mSOD mice throughout the disease course (11 weeks), including their levels of BM chimerism. Mice from **Group 5** (n=16) all exhibited stable GFP^+ BM engraftment that persisted to disease end-stage (Figures 4a and 4b). No differences were apparent in PBMC or BM GFP^+ levels in mSOD *vs*. control mice, so groups were formed according to the pre-conditioning BU dose received.

At one week post-transplant, GFP^+ cells comprised 8.8 ± 4.7% of total PBMCs in mice treated with 60 mg/kg BU (n=8), and 12.4 ± 5.4% in mice treated with 80 mg/kg (n=8), similar to our initial observations from Group 4. Week 4 GFP levels were also comparable, with 56.5 ± 5.5% PBMC chimerism observed in the 60 BU mice, and 64.3 ± 5.1% in the 80 BU group. After 8 weeks post-transplant, little difference was evident between the 2 dosages, with the 60 mg/kg group having 70.4 ± 4.3%, and the 80 group 74.3 ± 6.9% GFP^+ cells at this time. At end-stage, levels of GFP^+ cells suggest that chimerism in both groups would have increased further, had the mice survived for a longer duration. In the 60 mg/kg group, GFP proportions at 10 weeks were 73.9 ± 3.1% and increasing at disease endpoint (81.1 ± 3.4%). Similar results were found for the 80 mg/kg group, in which PBMC proportions were 78.7 ± 4.5% GFP^+ at 10 weeks and 83.3 ± 2.6% at endpoint. Upon analysis of the BM, the 60 mg/kg group was observed to be 75.09 ± 4.9% GFP^+, and the 80 mg/kg group almost identical at 74.5 ± 4.9%. While these results are just shy of what is considered to be high-level chimerism (≥80%), they suggest that low BU doses are as effective as higher doses in generating stable chimeric animals given adequate time.

Myeloid lineage cell reconstitution reached high levels by 3 weeks (84.2 ± 2.3% in the 60 mg/kg mice, and very high levels by 11 weeks post-transplant (95.0 ± 1.1%). In the 80 mg/kg group, high levels of GFP^+ myeloid cells were observed even earlier, at 2 weeks (86.8 ± 3.3%), and very high levels by 9 weeks (95.2 ± 1.5%), when they appeared to plateau (at end-stage; 95.9 ± 1.4% GFP^+).

It would seem that given time, dosages of 60 and 80 mg/kg BU are both capable of near complete reconstitution of the myelomonocytic compartment.

Lymphoid cell reconstitution was expectedly slow, and was the main reason the overall peripheral blood GFP^+ levels were not higher in the two treated groups. Levels greater than 50% were only observed after 4 weeks (51.4 ± 3.8%) in the 60 mg/kg group, and 3 weeks (50.8 ± 3.2%) in the 80 mg/kg. By 11 weeks, proportions of GFP^+ lymphocytes had progressively increased to over 75% in both groups (60 mg/kg; 76.7 ± 2.4%, 80 mg/kg; 81.2 ± 2.4%). Since BU exerts minimal effects on T and B lymphocytes (Bacigalupo *et al*., 2000), and the turnover of adaptive immune system memory cells is very slow, to the extent that some cells may persist for the life of the organism (Sallusto *et al*., 2004), it may be impossible to completely reconstitute the lymphoid compartment without some form of additional immunosuppression such as cyclophosphamide or whole-body irradiation. It is important to note that even though the transplanted GFP+ cells did not completely repopulate the animals, they did display typical myeloid and lymphoid lineage proportions (Muller-Sieburg *et al*., 2002) by approximately 5 weeks post-transplant onward (Figure 4c)

Figure 4a. Long-term myeloid and lymphoid reconstitution in B6 control and mSOD mice treated with 60 mg/kg freshly diluted Busulfan

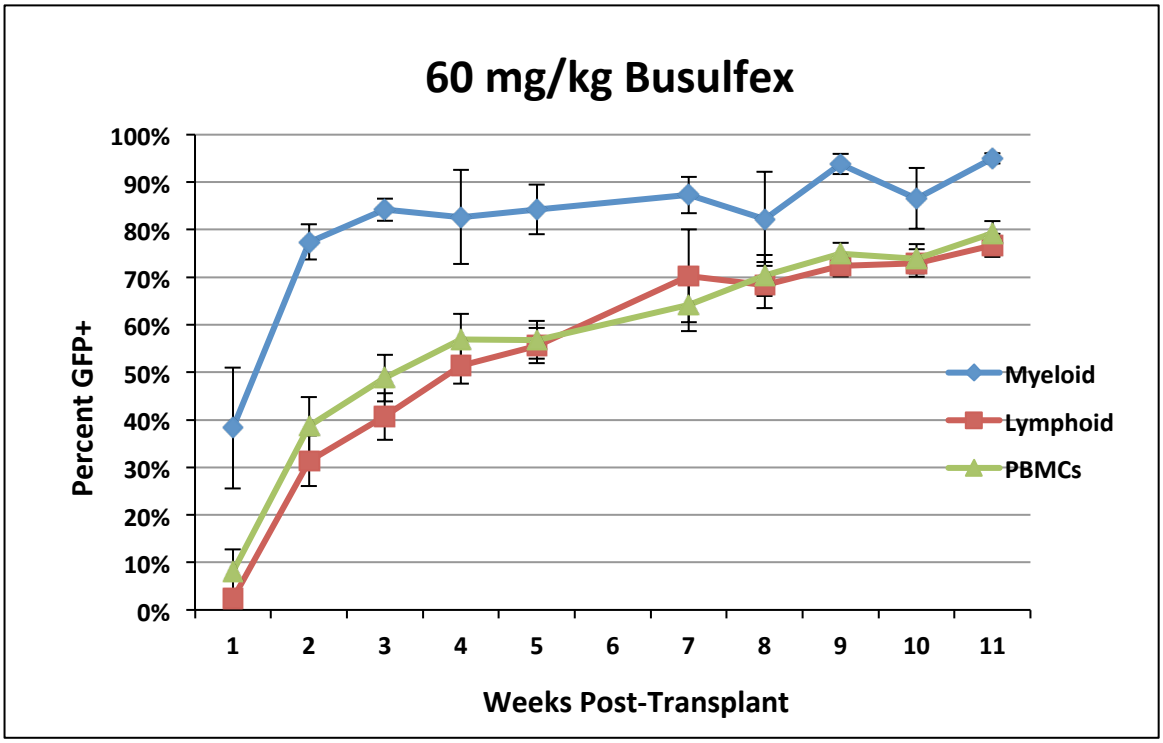

GFP PBMC chimerism increased slowly after 4 weeks with the 60 mg/kg dose, until reaching around 80% chimerism (≥80%) by 11 weeks post-transplant. Values were fairly consistent among all mice (n=8) throughout the collection period.

Figure 4b. Long-term myeloid and lymphoid reconstitution in B6 control and mSOD mice treated with 80 mg/kg freshly diluted Busulfan

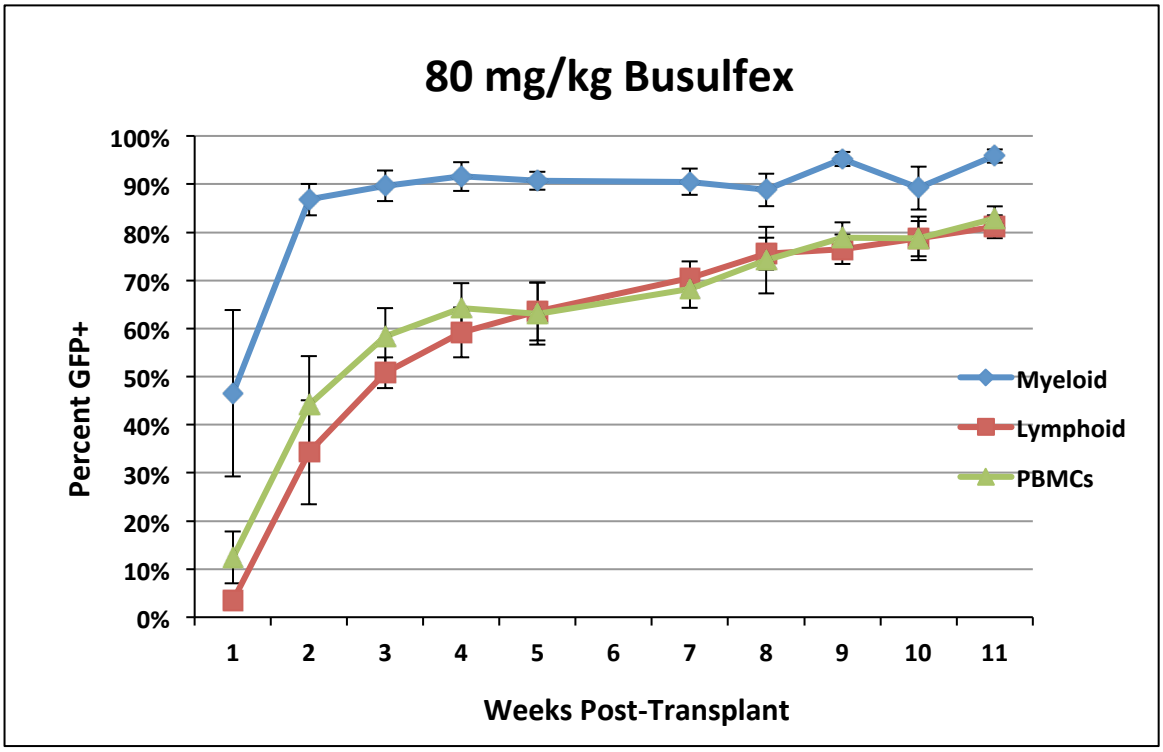

With 80 mg/kg BU, high-level chimerism was achieved, albeit after 11 weeks post-transplant.

Figure 4c. Lineage compositions of reconstituted GFP+ cells in C57Bl/6 mice treated with 60 and 80 mg/kg BU

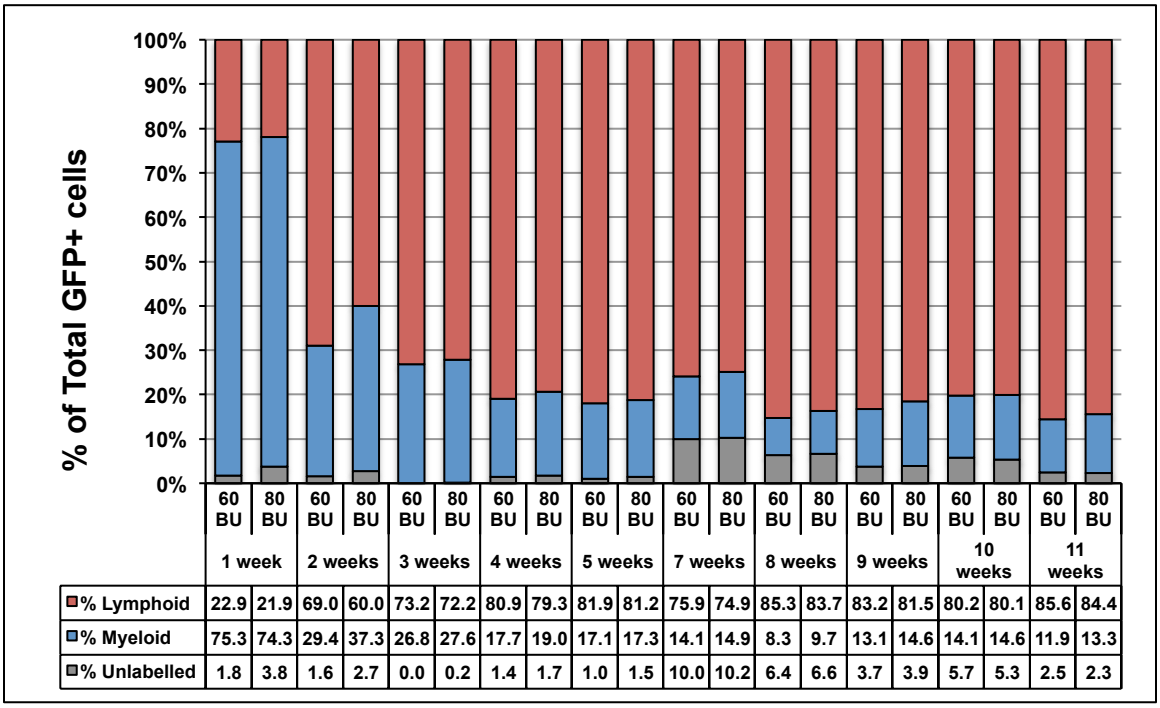

	60 BU	80 BU	60 BU	80 BU	60 BU	80 BU	60 BU	80 BU	60 BU	80 BU	60 BU	80 BU	60 BU	80 BU	60 BU	80 BU	60 BU	80 BU	60 BU	80 BU
	1 week		2 weeks		3 weeks		4 weeks		5 weeks		7 weeks		8 weeks		9 weeks		10 weeks		11 weeks	
% Lymphoid	22.9	21.9	69.0	60.0	73.2	72.2	80.9	79.3	81.9	81.2	75.9	74.9	85.3	83.7	83.2	81.5	80.2	80.1	85.6	84.4
% Myeloid	75.3	74.3	29.4	37.3	26.8	27.6	17.7	19.0	17.1	17.3	14.1	14.9	8.3	9.7	13.1	14.6	14.1	14.6	11.9	13.3
% Unlabelled	1.8	3.8	1.6	2.7	0.0	0.2	1.4	1.7	1.0	1.5	10.0	10.2	6.4	6.6	3.7	3.9	5.7	5.3	2.5	2.3

At week 1, most of the GFP+ cell population is made up of myeloid lineage cells. However by week 2, lymphoid cells begin to contribute a greater portion, which steadily increases throughout the 11-week collection period.

It has also been recognized that the potential for antigenic rejection of cells expressing the foreign GFP protein may play a role (albeit minor) in the lack of success we had with some of our transplanted mice. For this reason we tested supplementary immunosuppression with cyclophosphamide in **Group 6**. This was also done as BU is often used clinically together with cyclophosphamide. Out of the 4 mice treated, (n=1 control and n=3 mSOD) only two developed lasting chimerism. One mouse displayed symptoms of anaemia and liver complications and had to be euthanized. Another mouse had 64.5% GFP+

PBMCs at 1 week post-transplant but these were virtually non-existent by week 2. This mouse also had a large, persistent population of endogenous $CD3^+$ T cells (not present in the two successfully engrafted mSODs) suggesting that the CY-induced immunosuppression had little effect in this animal.

Of the mice that exhibited successful GFP cell re-engraftment, one displayed immediate high-level chimerism (86.4% GFP^+), while the other did not reach high levels until week 4. By this time, the average percentage of GFP^+ PBMCs was 97.3 ± 0.2% in both animals. Near complete myeloid reconstitution (97.2 ± 2.8%) was apparent in each mouse after 1 week, and remained stable until disease end-stage. GFP^+ lymphoid cell proportions on the other hand were initially low and variable (14.3 ± 14.7%), but rose to high levels (94.7 ± 3.7%) by 4 weeks post-transplant.

4.2. CNS Tissue

After BM transplantation, mSOD mice were allowed to progress to advanced stages of disease at which time spinal cords were collected and processed. Lumbar spinal cord sections were analysed for the presence of GFP^+ cells.

For mice in **Group 1** which did not exhibit successful donor chimerism, no GFP^+ cells were observed within the spinal cord.

Mice in **Group 2** that were successfully reconstituted with donor BM were observed to have GFP^+ cells in their lumbar spinal cords (Figure 5), while

unsuccessfully transplanted control and mSOD mice had no GFP$^+$ cells in their cords. These observations are quite similar to those seen in irradiation-induced BM chimeric mice (Lewis *et al*., 2009).

Figure 5. Presence of GFP$^+$ cells in the end-stage lumbar spinal cords of SJL/B6 control and mSOD mice treated with 100 mg/kg Busulfan

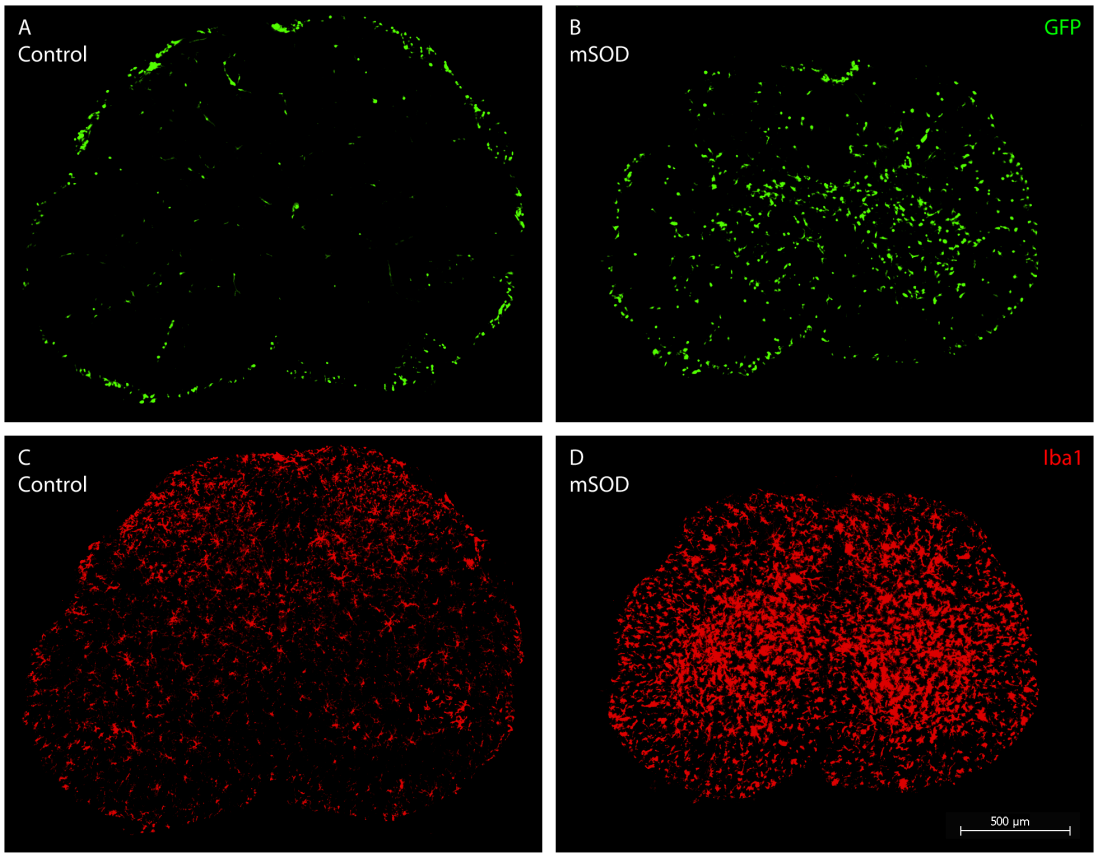

In control spinal cord, the majority of GFP$^+$ cells are observed in the surrounding meninges with very few present in the CNS parenchyma. (B) In mSOD mice, an increase in the number of GFP$^+$ cells can be seen compared to control. (C,D) Differential Iba1 immunoreactivity in control and mSOD mice, demonstrating increased Iba-1 cell number in mSOD spinal cord compared to control.

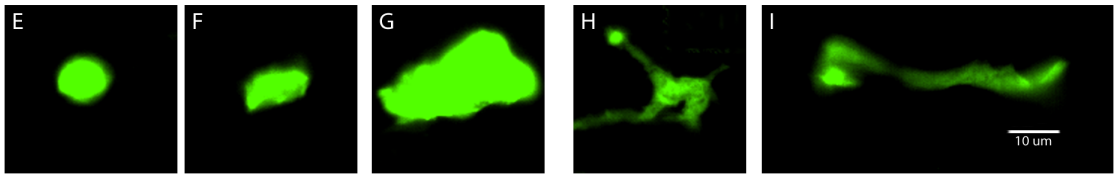

Donor cells were quantified and classified morphologically using a scheme developed by Vallieres and Sawchenko (2003). GFP^+ cells were categorized by round (E), rod-shaped (F) amoeboid (G) stellate (H) or elongated (I) morphology

GFP^+ cells in the 100 mg/kg treated SJL/B6 mice were observed to possess a variety of morphologies and were categorized as being round, rod, amoeboid, stellate or elongated in shape (Figure 5 E-I), as described in Vallieres & Sawchenko (2003). Categorizing cells based on morphology provides insight into their identity and function, when separation *via* histochemical means is difficult or impossible. In general, the stellate morphology is associated with parenchymal microglial cells, the elongated morphology with perivascular macrophages and the round morphology with T lymphocytes. The amoeboid and rod shapes are more difficult to assign to a particular cell population, but it is believed that they may represent macrophage or microglia that have acquired a phagocytic phenotype (Ransohoff & Cardona 2010), and the rod-shaped cells may be granulocytes or monocytic precursors (Audoy-Remus *et al*, 2008).

Control SJL/B6 mice displayed a large and variable number of GFP^+ cells (85.0 ± 33.3 cells/section; Figure 6), with a large proportion being of a round morphology (30.96 ± 13.6%), followed by an elongated phenotype (25.47 ± 6.3%) and then by rod-shaped cells (20.20 ± 7.5%). Comparatively, mSOD mice

had greater and more variable numbers of GFP^+ cells (330.1 ± 160.4 cells/section), most of which had a stellate morphology (29.61% ± 7.9%), followed by rod (24.07% ± 2.5%) and then elongated shaped cells (19.18% ± 5.7%) (Table 2). Although numerically, the mean cell number was larger in mSOD mice compared to controls, the groups were not significantly different due to the large variability in cell number in the mSOD group. These differential frequencies of morphological classes between control and mSOD mice likely reflect differences in the CNS microenvironment. In mSOD mice the advanced disease stages are associated with widespread microgliosis within the CNS and increased expression of inflammatory mediators which likely influence the differentiation of cells entering these tissues (Philips & Robberecht, 2011).

Figure 6. Numerical Comparison of GFP$^+$ cell entry in SJL/B6 control and mSOD lumbar spinal cords treated with 100 mg/kg Busulfan

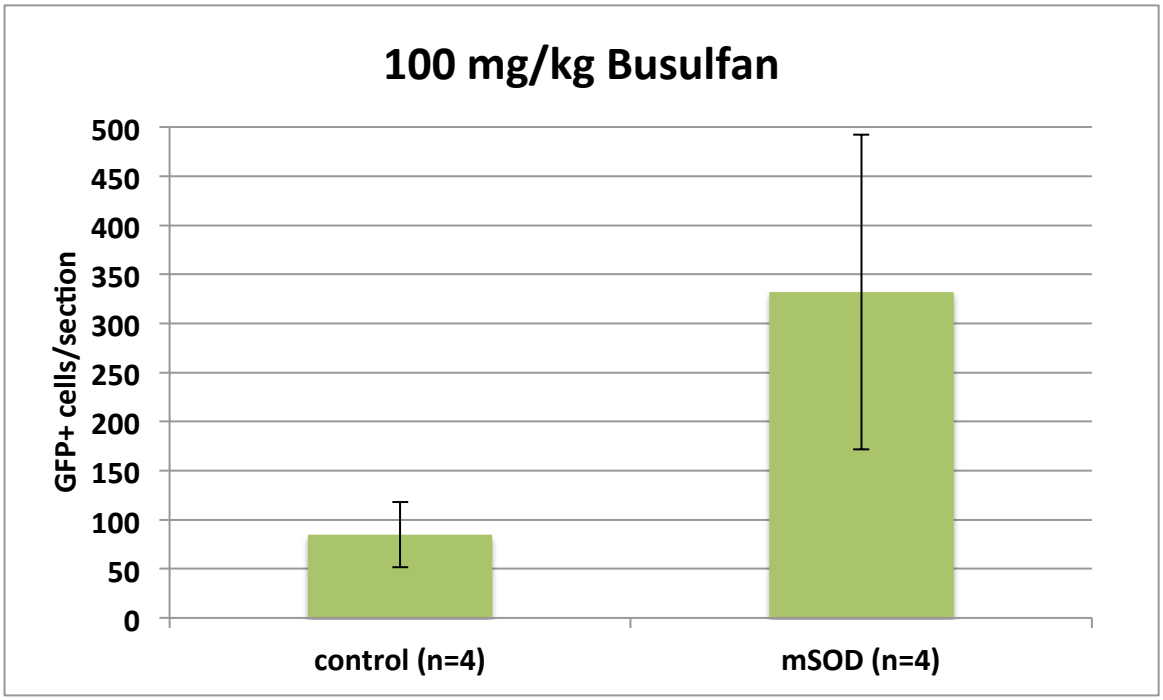

A greater number of GFP$^+$ cells was observed in the lumbar spinal cords of treated mSOD mice compared to controls. However, due to high variability in the experimental groups, especially the mSOD group, statistical significance was not achieved.

Table 2 – Morphological proportions of accumulating GFP$^+$ cells in allogeneically transplanted SJL/B6 mice treated with 100 mg/kg BU

	Average cells/sect. (mean ± s.e.)	**% round GFP cells** (mean ± s.e.)	**% rod GFP cells** (mean ± s.e.)	**% amoeb. GFP cells** (mean ± s.e.)	**% stellate GFP cells** (mean ± s.e.)	**% elong. GFP cells** (mean ± s.e.)
control (n=4)	**85.0 ± 33.3**	**30.96% ± 13.6%** (26.47 ± 14.00)	**20.20% ± 7.5%** (16.42 ± 7.50)	**4.02% ± 2.1%** (3.17 ± 1.91)	**19.35% ± 11.4%** (18.70 ± 17.70)	**25.47% ± 6.3%** (20.25 ± 3.94)
mSOD (n=4)	**332.1 ± 160.4**	**16.74% ± 11.1%** (65.67 ± 60.44)	**24.07% ± 2.5%** (77.37 ± 33.54)	**10.41% ± 4.0%** (38.58 ± 29.96)	**29.61% ± 7.9%** (93.50 ± 37.47)	**19.18% ± 5.7%** (57.00 ± 16.83)

mSOD mice exhibited a greater number of infiltrating GFP$^+$ cells in their lumbar cords, as well as a higher percentage of stellate-shaped cells; a morphology associated with parenchymal microglia.

Immunolabelling of mSOD lumbar spinal cords sections with antibody against the macrophage/microglial marker, Iba1, demonstrated a clear increase in the number of Iba1$^+$ cells and an increase in labelling intensity compared to control mice (Figure 5 C-D). We quantified the proportion of GFP$^+$ cells that express Iba1 as a function of cell morphology and averaged these values over 5 lumbar spinal cord sections from each mouse. These values were then averaged for each mSOD and control group. Across all morphological classes, the proportion of GFP$^+$ cells that expressed Iba1 was 25.1 ± 1.3% and 60.2 ± 9.3% in 100 mg/kg treated control and mSOD lumbar spinal cord sections, respectively. Of these, the majority (73.9 ± 16.1% and 87.0 ± 10.6%) of stellate-

shaped cells expressed Iba1 (Figure 7). This morphology as well as positive immunolabelling with Iba1, identifies these cells as BM-derived microglia.

Figure 7. Infiltrating GFP$^+$ cells immunolabel with Iba1 in mSOD SJL/B6 mice treated with 100 mg/kg BU

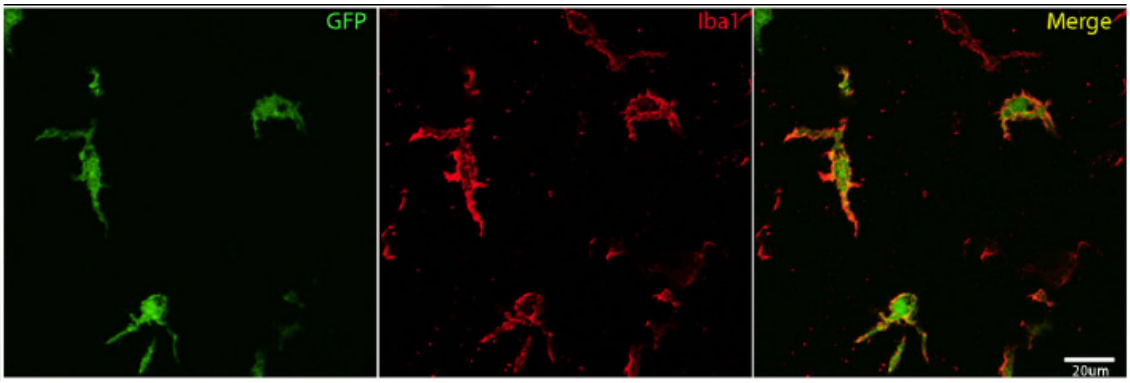

A portion of donor cells within the spinal cord of treated mice express the macrophage marker Iba1. Many of these cells also display the stellate morphology associated with parenchymal microglia.

Additionally, 5 lumbar sections from each 100 mg/kg treated mouse were immunolabeled with anti-CD3 antibody to identify and quantify the number of T cells within spinal cord sections. The numbers of T cells within mSOD and control lumbar spinal cords was highly variable among mice and when averaged over experimental groups, a substantial difference was observed, with 14.8 ± 15.2 and 60.4 ± 60.2 T cells per section observed in control *vs*. mSOD mice. This high degree of variability abrogated a statistically significant difference between groups. Although previous studies have observed increased numbers of T cells in the spinal cords of mSOD mice (Chiu *et al*., 2008), typically only a few T cells are observed in age-matched control spinal cords. There was also

considerable variability in the origin of T cells, with some mice primarily exhibiting donor-derived T cell populations within the spinal cord while in others T cells were primarily of host origin.

Sections were double labelled with CD3 and CD8 antibodies to classify the types of T cells populating the spinal cord. The majority of T cells (88.8 ± 5.1% in mSOD, 97.2 ± 2.5% in control mice) were $CD8^+$, identifying these cells as cytotoxic T cells (Figure 8). The presence of $CD8^+$ T cells within the CNS is often observed in association with a variety of types of encephalitis, ischemic lesions, and neurodegenerative diseases, including ALS, as well as in the CNS of the mSOD mouse. Only rarely are cytotoxic lymphocytes observed in the healthy CNS (Neumann *et al*., 2002). As BU readily crosses the BBB and its high-dose side effects include seizures and altered mental state (Hassan *et al*., 1996), the presence of $CD8^+$ T cells within the spinal cord of control mice treated with BU suggests that treatment at the dose employed has neurotoxic effects that may induce a neuroinflammatory response leading to T cell infiltration into the spinal cord.

Figure 8. Presence of Cytotoxic T-lymphocytes in the Busulfan treated spinal cord

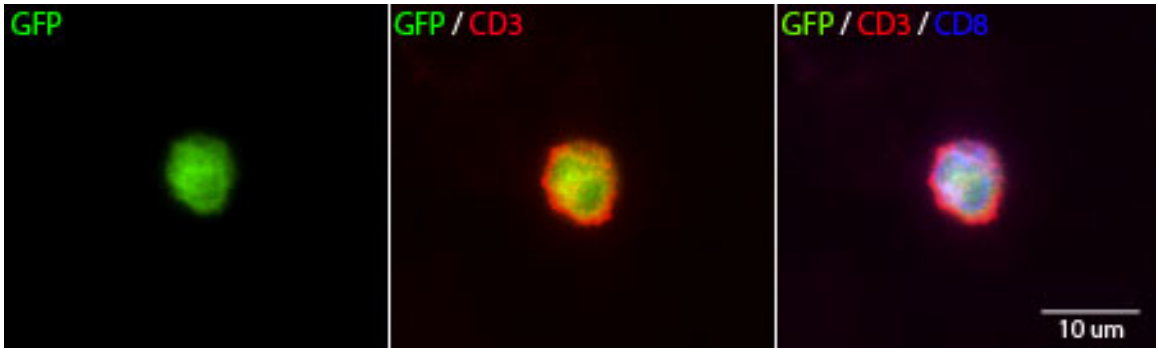

Variable numbers of T cells were observed in both control and mSOD SJL/B6 mice treated with 100 mg/kg BU. The majority of these $CD3^+$ cells co-immunolabelled with antibodies to CD8.

To analyse the kinetics of BM cell accumulation in the spinal cord, **Group 3** control SJL/B6 mice were sacrificed at 2 and 4 weeks post-BM transplant. In mice sacrificed a 2 weeks post-transplant (n=3), 1 mouse had unsuccessful re-engraftment, and the others exhibited variable numbers of GFP^+ cells in their lumbar spinal cords, with an average 3.4 cells per section in one mouse and 13.8 cells per section in another. The vast majority (88.2 ± 0.1%) of GFP^+ cells observed in the spinal cord were rod-shaped in morphology and were found in association with blood vessels. These cells did not label with Iba1 and only a portion (32.4 ± 12.4%) immunolabelled with the monocyte marker, CD11b. T cells were also observed within spinal cord sections at an average 3.0 ± 0.3 cells per section, numbers that are similar to those observed in control mice not treated with BU (Beers *et al.*, 2006).

Analysis of GFP^+ cell accumulation in the spinal cords of mice at 4 weeks (n=3) was again quite variable, with an average of 83.3 ± 37.0 donor cells per section. These cells were primarily round (47.0 ± 10.5%) or rod shaped (36.9 ± 1.4%) in morphology, with all GFP^+ round cells labelling for the ubiquitous T cell marker, CD3. Some of the rod cells again labelled with CD11b (46.7 ± 12.0%), and some also with Iba1 (45.6 ± 1.8%). Similar to the mice sacrificed at 2 weeks, almost all of these GFP^+ rod shaped cells were closely associated with the vasculature (91.0 ± 0.5%).

Although changing to syngeneic B6 recipient mice for our BMT experiments increased the effectiveness of our protocol, we observed much less cell entry into the spinal cords of these animals at early time periods. **Group 4** B6 control mice treated with 60 mg/kg BU (n=4), possessed only 1.5 ± 0.3 cells per section, 2 weeks BM post-transplant. All of these cells were of a rod-shaped morphology and were associated closely with the CNS vasculature. Similar results (3.9 ± 6.1 cells per section) at this time point were found for the group treated with 80 mg/kg BU (n=4), albeit with a higher cell number and with a large SEM, given that there was one mouse in the group with an average of 10 rod shaped cells per section as well as a few rare $Iba1^+$ elongated cells.

Figure 9. Numerical comparison of GFP$^+$ cell entry at 2 and 4 weeks in B6 control mice treated with 60 or 80 mg/kg Busulfan

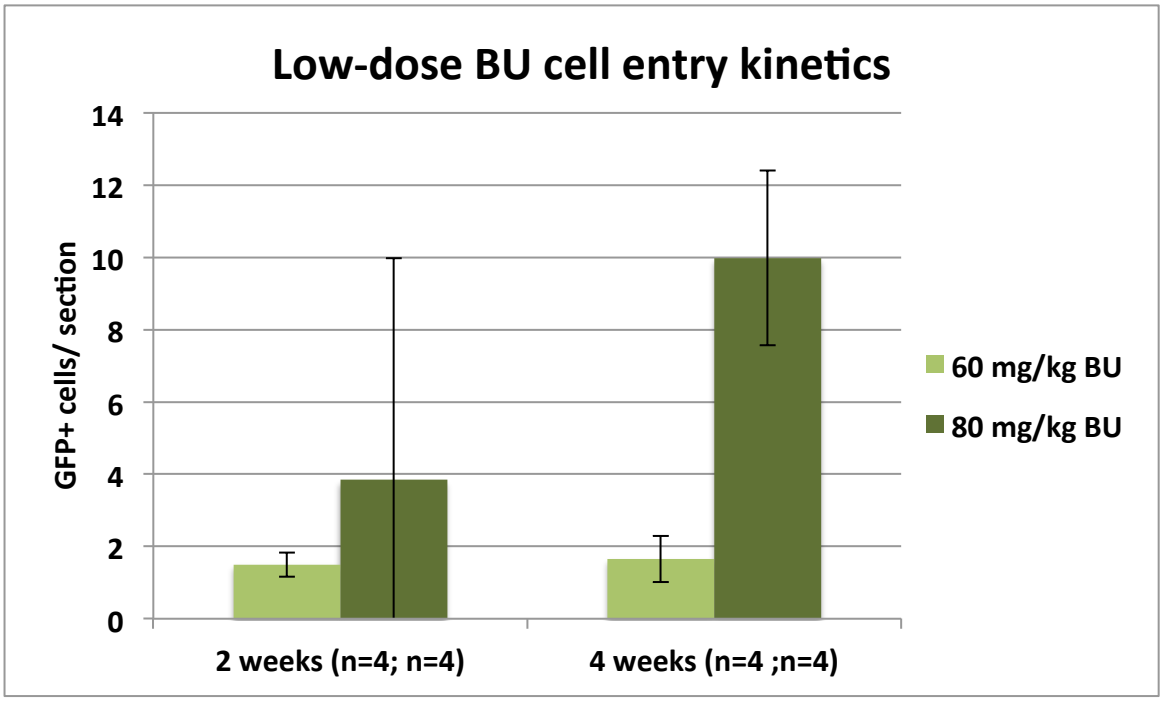

Limited numbers of GFP$^+$ cells were seen in control mice treated with 60 and 80 mg/kg BU at 2 weeks, and there was a trend for the cell number to increase marginally by 4 weeks. Due to variable infiltration in the 80 mg/kg group at 2 weeks, statistical significance was only obtained between 60 and 80 mg/kg at 4 weeks.

At 4 weeks there was almost no change in the number GFP$^+$ cells in the mice treated with 60 mg/kg, in comparison to what was seen at 2 weeks (Figure 9). These mice had 1.7 ± 0.6 GFP$^+$ cells per section, with all cells again being predominantly vascular-adjacent rod-shaped cells, some of which labelled weakly with CD68 (21.7 ± 16.5%) and CD11b (35.0 ± 21.2%). In the 80 mg/kg group at 4 weeks (n=4) there was an (albeit small) increase in the number of GFP$^+$ cells compared to 2 weeks. An average of 10.0 ± 2.4 cells per section was

observed in these mice, with a small portion (~15%) being made up of not only rod-shaped cells but stellate and elongated Iba1$^+$ cells as well. Akin to the 60 mg/kg 4 week group, there was some sparse labelling of the infiltrating rod cells with CD68 (13.2 ± 1.0%), Gr-1 (9.6 ± 7.6%) and CD11b (16.3 ± 5.3%). Unlike findings in our 100 mg/kg treated mice, mice from Group 4 at four weeks did not exhibit many CD3$^+$ T cells (1.2 ± 0.6), and none of these were CD8$^+$.

Figure 10. Donor-derived cells are evident in the CNS as early as 2 weeks post-transplant

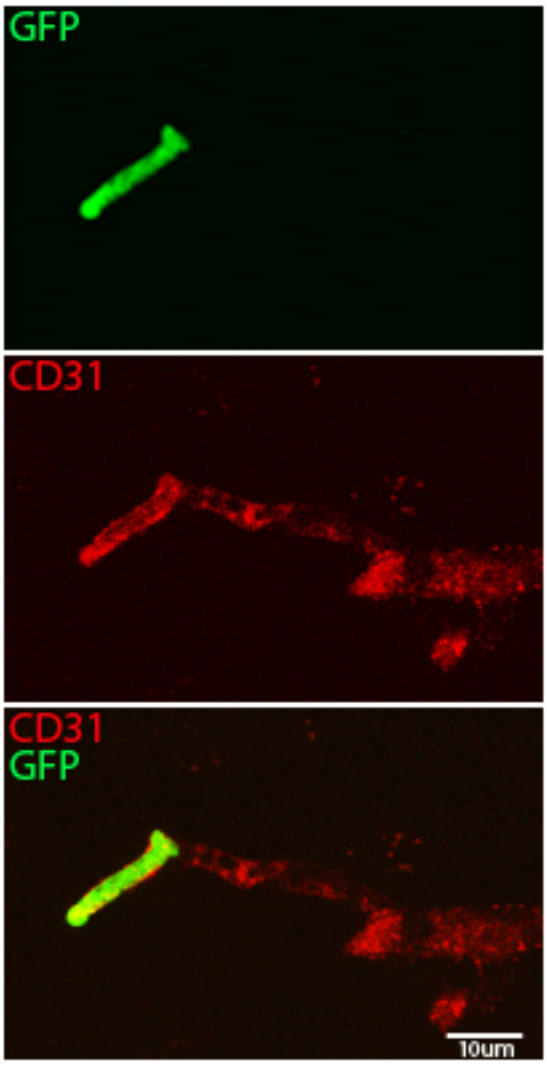

Mice pre-conditioned with 60 and 80 mg/kg BU exhibit exclusively rod-shaped cells GFP^+ cells at 2 and 4 weeks post-transplant. These cells associate closely with the CNS vasculature and label poorly with typical myeloid and lymphoid lineage markers, suggesting that they may be early progenitors or cells undergoing differentiation.

Control B6 mice from **Group 5** at 11 weeks post-transplant did not exhibit many more GFP^+ cells than what was seen at 4 weeks in group 4 (Figures 11

and 12, and Table 3). Controls treated with 60 mg/kg BU (n=4) possessed an average of 7.7 ± 3.9 cells at end-stage, with the vast majority being rod-shaped (65.5 ± 8.3%), followed by an elongated morphology (20.6 ± 14.2%). In the 80 mg/kg control group (n=4) numbers were slightly higher, with an average cell per section count of 12.8 ± 4.5, and proportions of rod-shaped cells being slightly less (53.1 ± 4.4%) and those of elongated cells slightly more (36.8 ± 10.8%).

Figure 11. Presence of GFP$^+$ cells in the end-stage lumbar spinal cords of B6 control and mSOD mice treated with 60 or 80 mg/kg Busulfan

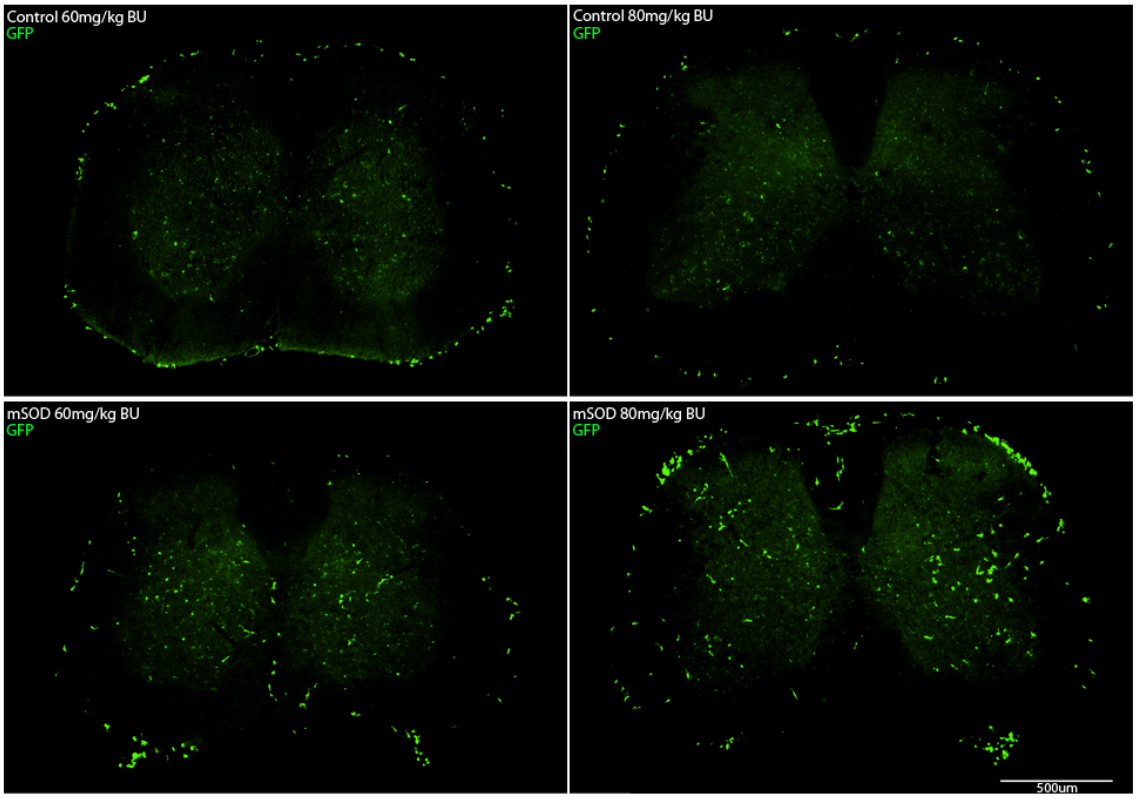

GFP$^+$ cells accumulate in the grey and white matter of lumbar spinal cord sections, especially in the surrounding leptomeninges at 11 weeks after transplantation following BU treatment (60mg/kg shown on the left, 80mg/kg on the right). Significantly greater numbers of BMDCs accumulated in mSOD lumbar spinal cords (lower panels) compared to age-matched controls (upper panels)

Figure 12. Numerical Comparison of GFP$^+$ cell entry at end-stage in B6 control and mSOD lumbar spinal cords treated with 60 or 80 mg/kg BU

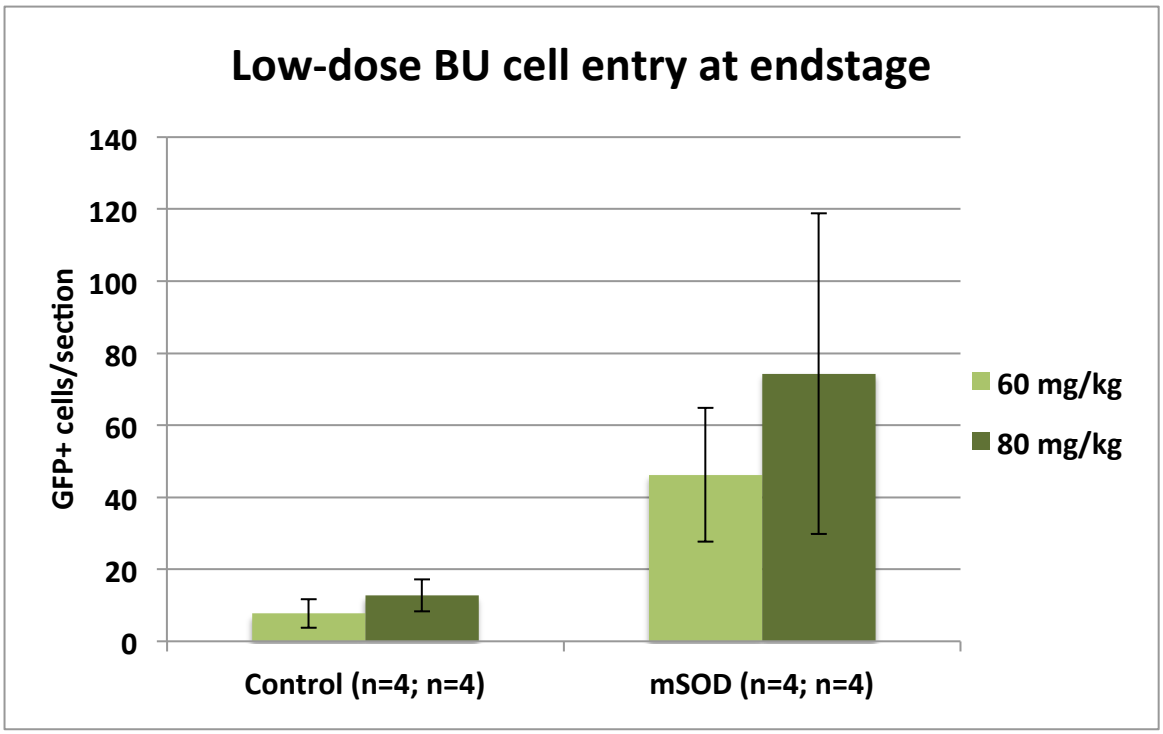

Statistically greater numbers of GFP$^+$ cells were present in mSOD spinal cords at end-stage compared to controls, however there was no significance difference in GFP$^+$ cell number in CNS between the 60 mg/kg and 80 mg/kg dose.

mSOD mice in both the 60 mg/kg (n=4) and 80 mg/kg (n=4) groups, while exhibiting significantly greater numbers of infiltrating cells than controls, also displayed considerable variability. The 60 mg/kg mSOD group, had 46.2 ± 18.6 cells per section, while the 80 mg/kg group had 74.3 ± 44.5 cells/section. The proportions of each cell type were again different in these animals compared to controls. In the lower dose group, 39.3 ± 5.5% of the GFP$^+$ cells were elongated,

29.4 ± 2.8% were rod-shaped, and 18.0 ± 9.0% were stellate. Similarly, the 80 mg/kg group was 41.5 ± 6.3% elongated, 29.8 ± 4.3% rod-shaped, and 22.0 ± 10.3% stellate. In these mice, all of the stellate and amoeboid-shaped GFP^+ cells also labelled with Iba1, and ≥99% of the elongated cells were $Iba1^+$ in both the 60 and 80 mg/kg groups. Rod-shaped cells, although they made up a large proportion of the infiltrating GFP^+ cells, had variable Iba1 expression. In the 60 mg/kg group, 71.5 ± 9.3% of the rod cells were $Iba1^+$, whereas in the 80 group, 83.3 ± 12.5% labelled positively. As in other groups examined, no round shaped cells labelled with Iba1 or other macrophage markers.

Figure 13. End-stage mSOD and age-matched control mice treated with 60 and 80 mg/kg exhibit vascular-associated elongated cells

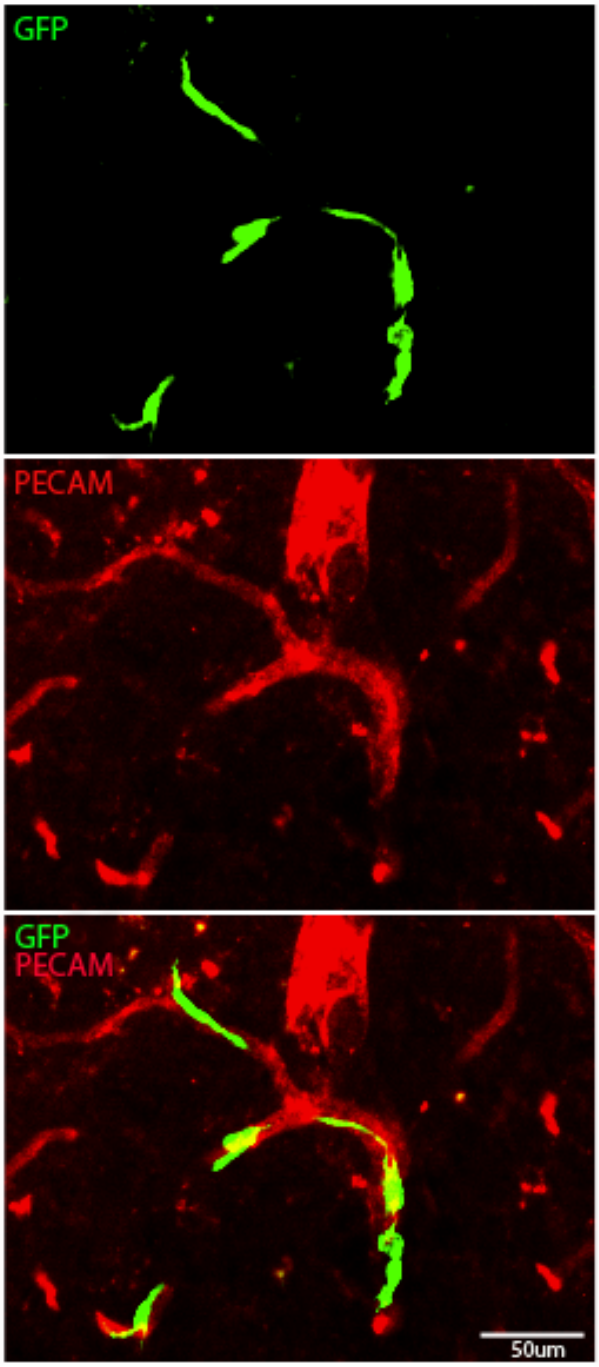

The presence of elongated cells at later time points corresponds with reported turnover time typical for perivascular macrophages, and also suggest that rod-shaped haematopoietic lineage cells are the immediate precursors to CNS-associated macrophage.

Table 3 – Morphological proportions of accumulating GFP$^+$ cells in syngeneically transplanted B6 Mice treated with 60 and 80 mg/kg BU examined 11 weeks post-transplant

	Average cells/sect. (mean ± s.e.)	**% round GFP cells** (mean ± s.e.)	**% rod GFP cells** (mean ± s.e.)	**% amoeb. GFP cells** (mean ± s.e.)	**% stellate GFP cells** (mean ± s.e.)	**% elong. GFP cells** (mean ± s.e.)
60 mg/kg control (n=4)	**7.7 ± 3.9**	**10.11% ± 6.32%** (0.67 ± 0.49)	**65.46% ± 8.31%** (4.98 ± 2.52)	**1.83% ± 0.37%** (0.15 ± 0.10)	**2.01% ± 3.19%** (0.67 ± 0.49)	**20.61% ± 14.24%** (1.67 ± 1.58)
60 mg/kg mSOD (n=4)	**46.2 ± 18.6**	**10.86% ± 7.98%** (4.52 ± 2.76)	**29.35% ± 2.76%** (13.22 ± 4.03)	**2.52% ± 0.84%** (1.22± 0.73)	**17.99% ± 8.95%** (9.52 ± 8.63)	**39.30% ± 5.45%** (17.68 ± 5.44)
80 mg/kg control (n=4)	**12.8 ± 4.5**	**4.87% ± 3.38%** (0.67 ± 0.61)	**53.13% ± 4.42%** (6.82 ± 2.71)	**1.70% ± 0.52%** (0.20 ± 0.00)	**3.56% ± 4.96%** (0.62 ± 0.97)	**36.84% ± 10.80%** (4.48 ± 1.30)
80 mg/kg mSOD (n=4)	**74.3 ± 44.5**	**4.76% ± 2.25%** (2.85 ± 1.33)	**29.75% ± 4.25%** (21.07± 11.69)	**2.00% ± 1.64%** (1.95 ± 2.59)	**21.95% ± 10.33%** (19.63 ± 17.39)	**41.54% ± 6.31%** (28.75 ± 13.28)

mSOD mice again exhibited a greater number of infiltrating GFP$^+$ cells in their lumbar cords, as well as a higher percentage of elongated and stellate-shaped cells.

Due to the large number of T lymphocytes we observed in both Groups 2 and 3 treated with 100 mg/kg, we wanted to see if a similar effect was observed with the lower dosages of 60 and 80 mg/kg. Sections were again labelled with anti-CD3 and anti-CD8 antibodies to detect the presence of T cell populations in the lumbar spinal cord. In control BU mice, CD3$^+$ T cell numbers were

comparable to age-matched untreated controls, which possess an average of 3.2 ± 1.8 $CD3^+$ cells per section (Figure 12, Table 4, unpublished data). At 60 mg/kg, 4.9 ± 3.8 T cells per section were observed, and at 80 mg/kg, 3.7 ± 1.9 cells. Of these T cells, a small few labelled positively for CD8, 0.9 ± 0.9 from the 60 BU group and 0.5 ± 0.4 from the 80 BU group (Figure 14). This suggests that the drug may produce mild inflammation, even at these low doses, as it is unusual to see any $CD8^+$ T cells in the CNS of control mice.

Figure 14. Numerical Comparison of T Lymphocytes in end-stage B6 control and mSOD lumbar spinal cords treated with 60 or 80 mg/kg BU

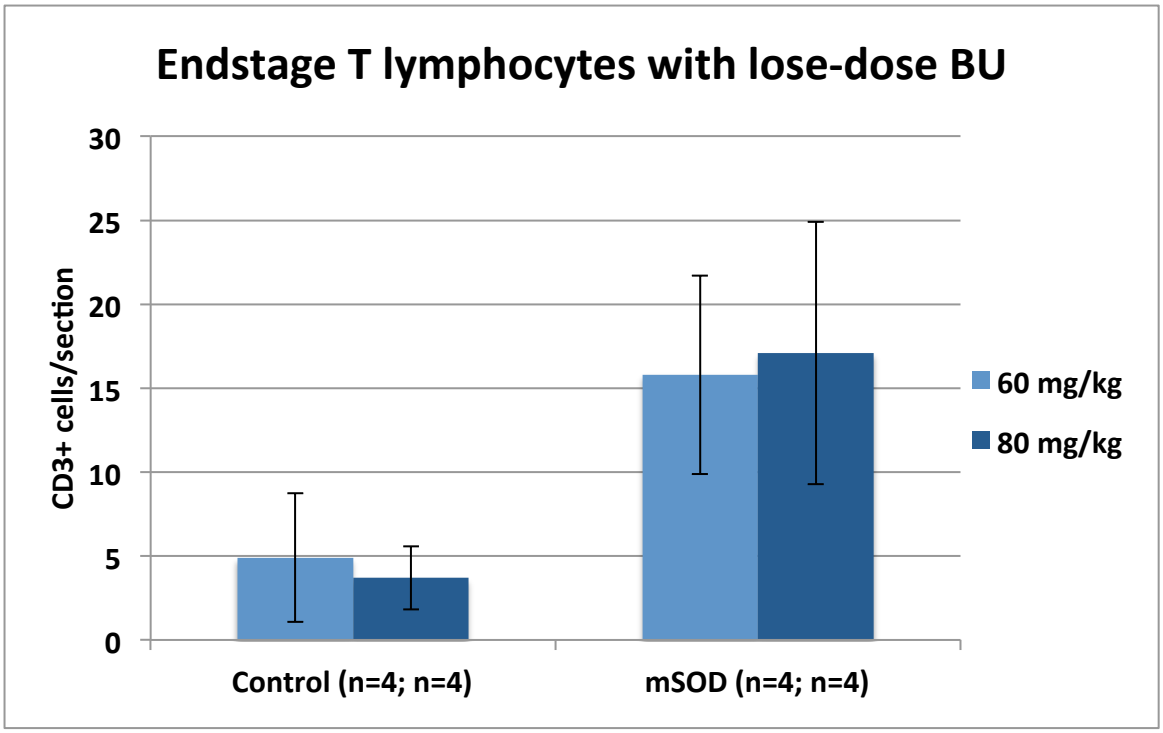

T lymphocyte numbers in mice treated with 60 and 80 mg/kg BU appeared similar to end-stage mSOD and age-matched controls.

Table 4 – Numerical comparison of cytoxic T-lymphocyte numbers at different time points in control and mSOD mice

Age	**Control** (n=4 for each time point)		**mSOD** (n=4 for each time point)	
	CD3$^+$ (mean ± s.e.)	**CD8$^+$** (mean ± s.e.)	**CD3$^+$** (mean ± s.e.)	**CD8$^+$** (mean ± s.e.)
11 weeks	**2.6 ± 1.5**	None	**10.8 ± 5.4**	None
15 weeks	**3.5 ± 0.4**	None	**13.2 ± 7.1**	None
End-Stage	**3.2 ± 1.8**	None	**29.3 ± 11.7**	**18.1 ± 6.1**

CD8$^+$ cytotoxic lymphocytes are only observed in the CNS of the mSOD mouse at advanced disease stages.

In the mSOD groups, numbers were more consistent than in the 100 mg/kg treated mice. In the 60 mg/kg mice, 15.8 ± 5.9 T cells per section were observed, of which 4.2 ± 1.3 per section were also CD8$^+$. In the 80 mg/kg group, 17.1 ± 7.8 T cells per section were seen, with 6.6 ± 3.8 of these per section co-labelling for CD8. These results, although less than what is typically seen in untreated mSOD mice at endstage (Figure 15, Table 4), were comparable in terms of the ratio of CD8$^+$ cells to total CD3 T cells. The absolute numbers were unexpected, however, given the extreme number of CD8$^+$ cells seen in the 100

mg/kg SJL/B6 mice, but they suggest that employing lower doses may help to account for the abnormal influx of $CD8^+$ cells that occurs with higher dose BU treatment.

Figure 15. Numerical comparison of T Lymphocytes in pre-symptomatic, symptomatic and end-stage control and mSOD lumbar spinal cords

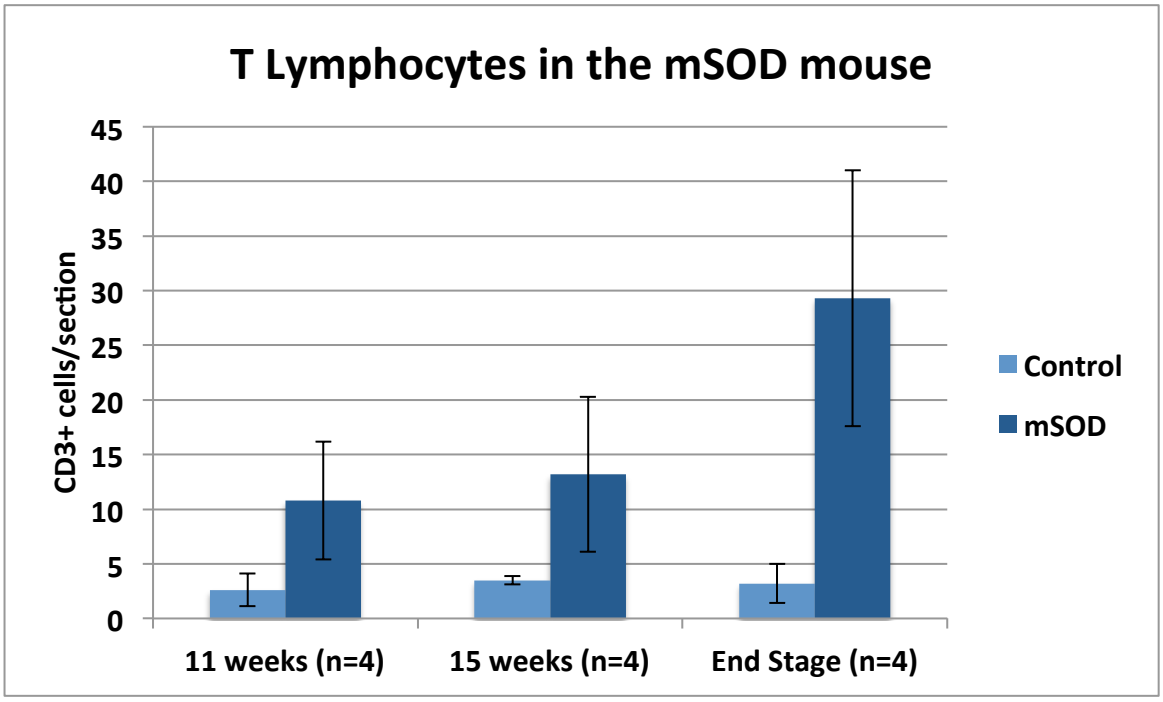

Infiltrating T cell numbers increased with disease progression in the mSOD mouse, whereas numbers in age-matched controls were stable.

Of the 2 out of 4 SJL/B6 mice treated with 80 mg/kg BU and 200 mg/kg CY from **Group 6** exhibiting successful chimerism, both were mSOD animals, and both exhibited a large number of GFP^+ cells in their spinal cords at end-stage. These animals had on average 359.3 ± 24.0 cells per section, which was comparable to the number of cells observed in mSOD mice treated with 100

mg/kg BU (Table 2). These mice possessed a large proportion of stellate-shaped GFP^+ cells, (39.4 ± 1.2%) as well as elongated GFP^+ cells (25.2 ± 0.5%), all of which were $Iba1^+$. Rod cells were also commonly observed, however only (69.2 ± 3.5%) of these co-labelled with $Iba1^+$. T cell numbers were more variable than seen with 100 mg/kg BU alone, with one mouse having an average of 64.0 $CD3^+$ cells per section, and the other only 21.4 T lymphocytes per section. $CD8^+$ numbers were also variable; the first mouse had a mean of 13.0 cytotoxic lymphocytes per section, while the other had only 1.4 per section.

5. DISCUSSION

Here we present evidence that BU, a chemotherapeutic agent, is capable of inducing successful engraftment of donor BM cells, as well as promoting significant cell entry into the CNS. Although this has been inferred previously by the work of Yeager *et al*., (1993) this is the first time haematopoietic cells have been shown to take up residence in the CNS without the application of ionizing irradiation.

5.1. Busulfan-Generated Chimeric Mice

The current literature contains several reports of inconsistent chimerism generated with a variety of BU pre-conditioning doses. Doses as low as 20 mg/kg, followed by injection of 15 million BM cells have been reported to occasionally produce chimerism of up to 40%, albeit 62 weeks after transplantation (Andersson *et al*., 2003). Chimerism greater than 80% has also been observed as early as 13 weeks post-transplant, with pre-treatments as low as a single 40 mg/kg bolus and injection of 20 million BM cells (Hsieh *et al*., 2007). As I expected that there would be a dose-dependent relationship between the extent of pre-conditioning and the level of BM engraftment (Nevozhay & Opolski, 2006), and given the lifespan of the mSOD mouse, we

chose to begin treatment with a higher BU dosage than is normally utilized in other sub-myeloablative BU studies.

Initially we employed a dosage of 80 mg/kg and gave SJL/B6 mSOD mice a bolus of 500,000 5-FU-enriched bone marrow cells, as there had been reports of rapid reconstitution with this protocol in the unpublished results of Barry (2003). However we did not observe the presence of GFP^+ cells with this procedure, in either the peripheral blood or the BM compartment.

In the next trial, we attempted to obtain chimerism by using a larger dose of BU, and providing mice with a much larger, albeit non-enriched, quantity of GFP^+ BM cells. Although 100 mg/kg given as five successive 20 mg/kg injections is a much higher dose then that utilized by others (Yeager *et al*., 1993; Andersson *et al*., 2003; Hsieh *et al*., 2007), it is still below the maximum tolerated dose of 150 mg/kg for mice (Mauch *et al*., 1988), which equates to approximately 70% of the high-dose typically given to humans undergoing stem cell transplantation (Andersson *et al*., 2003). In terms of the BM transplant cell number delivered, we thought that 30 million cells was higher than the usual amount transplanted, but we wanted to ensure the success of our protocol.

Nonetheless, even with these alterations, we only obtained reconstitution in a portion of the SJL/B6 mice we treated. One possibility for the lack of success of the BU myeloablation was the stability of BU when diluted with PBS and kept as a stock solution. Although not mentioned in the drug information

package for BU (Otsuka Pharmaceuticals), it has been reported that the potency of the drug when diluted is greatly diminished in just 8 hours (Jopling & Rosendaal, 2001).

For this reason, the mice in our next experiment were treated with BU that was diluted just before administration. Freshly diluted BU appeared to increase the effectiveness of our protocol, as 83% of our mice exhibited successful engraftment, compared to 32% with the original protocol. Myeloid cell reconstitution was nearly complete in these animals by 2 weeks, and BM analysis at this time point revealed approximately 60% chimerism. Lymphoid cells initially lagged behind in terms of their reconstitution, but by 4 weeks they also exhibited high levels in the peripheral blood. The rapid turnover of myeloid cells and the slow reconstitution of lymphoid cells is a commonly reported feature of BU treatment (Anam *et al*., 2006; Hsieh *et al*., 2007), presumed to be due to the mildly immunosuppressive nature of the drug and the short half-life of monocytic and granulocytic cells. In any case, I observed that GFP^+ BM populations reached levels of approximately 90% by 4 weeks with 100 mg/kg BU, combined with the fact that there were no fatalities related to treatment toxicity, suggesting that moderate-dose BU treatment is an effective and efficient way to generate rapid BM chimerism.

Another reason for the variable success that I had with generating consistent BU chimeras, may be due to incompatible MHC alloantigens between our donor and recipient mice. MHC type I and II surface antigens can greatly

influence transplant acceptance or rejection in allogeneic transplants. MHC class I and II antigens comprise 11 molecules and are commonly referred to as 'H-2 antigen' in mice (Snell *et al*., 1964). MHC I encompasses the H-2D, H-2K and H-2L molecules, and is expressed under physiological conditions on almost all nucleated cells (neuronal cells being an exception). MHC I plays an important role in the recognition of non-self antigen, such as peptides in virally infected or tumorigenic cells, as they present these to $CD8^+$ cytotoxic T cells. MHC II encompasses the H-2A and H-2E molecules, and these are mainly expressed on antigen presenting cells (APCs) such as macrophages. MHC II is involved in presenting phagocytised and processed peptides to $CD4^+$ T cells. As MHC molecules are very polymorphic, each strain of laboratory mouse is homozygous and can be defined by its MHC haplotype (Fischer-Lindahl, 1997). A small uppercase letter beside each H-2 subclass generally designates the haplotype of a strain. The SJL MHC haplotype antigens are $H\text{-}2K^s$, $H\text{-}2D^s$, $H\text{-}2L^s$, $I\text{-}A^s$ and $I\text{-}E^{null}$, whereas the B6 haplotype is $H\text{-}2K^b$, $H\text{-}2D^b$, $H\text{-}2L^{null}$, $I\text{-}A^b$ and $I\text{-}E^{null}$. This means a mixed-strain SJL/B6 mouse could potentially have any combination of these alloantigens, and T lymphocytes specific for that type, which might lead to rejection of transplanted donor cells if they are recognized as foreign.

To see if this was the case with our mice, we exclusively transplanted mice on a B6 background to match the strain of our GFP donor mice in groups 4 and 5. We also wanted to explore the kinetics of lower dose BU engraftment and attempt to account for the Iba immunoreactivity and $CD8^+$ T cell influx that we

saw with 100 mg/kg. Additionally, we reduced the volume of transplanted GFP^+ cells from 30 million to 15 million. The reason for this reduction in cell number was to make the protocol more comparable to the dosages used previously in the literature.

It would seem that the major factor limiting our consistent generation of BU induced chimeric animals was rejection of transplanted cells expressing alloantigen unfamiliar to the host animal. Even when we employed a protocol with lower dose BU (60 and 80 mg/kg) and donor fewer cells than in our previous experiments, we still achieved stable engraftment in every syngeneic transplant we preformed (n=32). With our first B6 group of transplants (group 4), we were able to show that greater than 50% blood chimerism is possible 4 weeks after pre-treatment with 60 mg/kg BU before BMT, and by 2 weeks with 80 mg/kg BU. Both these groups of mice also displayed rapidly increasing GFP^+ myeloid cell populations, in excess of 70% by 4 weeks time, which is one of the best indications of successful stem cell engraftment.

The second group (group 5) of mice transplanted in this manner were mSOD control pairs aged 6 weeks, and as such, allowed successive blood sampling for 11+ weeks post-transplant before disease manifestation in the transgenic animals. We were able to observe the kinetics of reconstitution with 60 and 80 mg/kg for much longer in these cases, and also confirm our short-term results from group 4. With the 60 mg/kg dose, GFP^+ peripheral blood cells made up ~40% at 2 weeks, and ~55% at 4 weeks, in both groups 4 and 5. With 80

mg/kg, results from group 4 and 5 were consistent, with ~65% of cells being GFP^+ at 4 weeks. Past this time point, weekly increases in blood chimerism appeared to taper off, until they reached stable levels. In these mice we also saw near identical GFP blood levels at end-stage, with the 60 mg/kg BU group displaying 81.1 ± 3.1% blood chimerism and 75.1 ± 4.9% BM chimerism, and the 80 mg/kg group possessing 83.3 ± 2.6% blood chimerism and 74.5 ± 4.9% BM chimerism. These results are akin to the work of Hsieh *et al*., (2007) where ~80% blood chimerism was shown at 13 weeks after a low dose of BU and 20 million BM cells.

Although our last group treated with 80 mg/kg BU and additional 200 mg/kg CY was small, and only half of the treated animals demonstrated lasting GFP chimerism, it was nonetheless interesting to observe the relative similarity in reconstitution between these mice and those treated with 100 mg/kg BU. Both exhibited similar GFP chimerism early on at 2 weeks (100 BU; 81.6 ± 13.3%, 80 BU + 200CY; 85.1 ± 16.5%) and later at 4 weeks (100 BU; 97.5 ± 0.4%, 80 BU + 200CY; 97.3 ± 0.2%). Myeloid reconstitution was extremely rapid in both groups, and lymphoid reconstitution slow until 3 weeks time. This suggests that both regimens are capable of inducing very high-level chimerism by 4 weeks post-transplant, and also that even with extensive immunosuppression, lymphoid reconstitution requires at least 3 weeks to reach substantial levels, which is consistent with the literature (Mosley & Klein, 1992).

5.2. Donor Cell Accumulation in The Lumbar Spinal Cord

Previous studies by our lab have shown that greater numbers of transplanted haematopoietic cells accumulated in the spinal cord of irradiation-induced chimeric mSOD mice compared to controls (Solomon *et al*., 2006; Lewis *et al*., 2009). With lethal irradiation (9-10Gy), 69.6 ± 6.7 (n=4) GFP^+ cells per section were observed in SJL/B6 control mice, and 431.7 ± 42.3 (n=4) cells were observed in age-matched mSOD mice, demonstrating an 5-7 fold greater BMDC accumulation in these animals. These studies also demonstrated that the large increase in BM-derived CNS cells seen in these mSOD animals is not a consequence of strain mis-matching as it was shown that GFP^+ cell accumulation was approximately equal for both SJL/B6 and B6 strains.

Mean GFP^+ cell accumulation in our SJL/B6 mice treated with 100 mg/kg BU (control; 85.0 ± 33.3, mSOD; 332.1 ± 160.4) was similar to what we have seen in lethally irradiated animals (above), in that there is an increase in mSOD mice compared to controls. The cell numbers were more variable, especially in the mSOD group, and prevented statistical significance from being obtained between control and mSOD mice for the 100 mg/kg BU group. There was a roughly 4-fold increase in mean cell number between mSOD and WT mice. This is somewhat smaller than typically seen when using irradiative myeloablation (Solomon *et al*., 2006). The large range (~45-125 GFP^+ cells/section) seen in controls, and in mSOD spinal cords (~130-495 GFP^+ cells) may have been a

consequence of the bioavailability of BU in these experiments as I did not use freshly prepared BU for the earlier groups and I am now aware that there is limited shelf-life of BU once it has been diluted with PBS. Given that our 100 mg/kg mice were treated with BU that had been diluted and stored for differing periods of time, it would be reasonable to assume that this played a role in the variable cell accumulation seen. However, it is important to point out that the blood chimerism observed in all of the successfully transplanted animals was similar suggesting that this variability in GFP^+ cell accumulation might be due to the genetic diversity inherent in the hybrid SJL/B6 line.

The frequency with which different morphologies of BMDC are observed in control and mSOD animals may be a reflection of the state of their respective CNS microenvironments. In the control spinal cords, there were relatively large frequencies of round and elongated cell morphologies that correlate well with absolute numbers of donor-derived $CD3^+$ T lymphocyte and perivascular macrophages, respectively. Whereas, in the mSOD spinal cords, ~30% of GFP^+ cells were stellate in morphology, and ~80% of these also labelled with $Iba1^+$ suggesting the phenotype of BM-derived parenchymal microglia. The two differential forms of inflammation occurring in each respective group suggests that in the control mice, there is only inflammation and endothelial activation produced by BU crossing the blood-brain barrier (Zeng *et al*., 2010), whereas in the mSOD mice there is additional microgliosis and neurodegeneration associated with the underlying disease.

In experiments evaluating changes in GFP^+ cell number with time, I observed only 1.5 ± 0.3 GFP^+ cells in the CNS of mice 2 weeks after transplant. However, GFP^+ rod cells were apparent as early as 10 days after transplantation (Figure 10). The appearance of this cell type within the first two weeks following transplantation is consistent with the findings of Audoy-Remus *et al*., (2008). This group reported that these early 'rod-shaped' cells are often Gr-1^+ granulocytes or $CD11b^+$ monocyte precursors, which may go on to differentiate into perivascular macrophages. We attempted to label these cells in a similar manner, but found that only a few labelled weakly with Gr-1, and only a third demonstrated CD11b labelling. Caution must be used when making direct comparisons between our data evaluating spinal cord tissue following BU in mSOD and wildtype mice, and the data of Audoy-Remus *et al*., which studied cortical tissue following irradiation-induced myeloablation as depleting and repopulating perivascular macrophages with anti-angiopoietin-2 may be completely different from what occurs with pre-conditioning and BMT.

In this group at 4 weeks, we saw a large number of GFP^+ cells (83.3 ± 37.0 per section) with 100 mg/kg. These cell numbers, although again variable, are very similar to what we saw with 100 mg/kg in end-stage age-matched control SJL/B6 mice (85.0 ± 33.3). This time point seems to be characterised by appearance of rod-shaped cells that label poorly with $Iba1^+$ and $CD11b^+$, as well as $CD3^+$ T cells, which would seem to suggest that most of the cell entry occurring in BU-treated control mice arises early on, in the 3-4 week post-

transplant time period. It also suggests the possibility that further entry/expansion of what are potentially monocytic precursors, may be secondarily influenced by T lymphocytes.

The experiments examining cell accumulation shortly after transplantation with syngeneic B6 mice yielded similar results at 2 weeks to what we saw with the SJL/B6 mice at the 100 mg/kg dose, with few cells present in the spinal cord at this time. However our 4 week results were significantly lower than what we observed previously in Group 3; there were only 1.7 ± 0.6 cells/section with 60 mg/kg BU, and 10.0 ± 2.4 cells with the 80 mg/kg, much less than the 83.3 ± 37.0 cells we saw with 100 mg/kg. These rod-shaped cells labelled poorly with a variety of myeloid cell markers (Iba1, CD68, Gr-1, CD11b), suggesting that they may be early progenitors or cells undergoing differentiation. We also did not observe any sort of abnormal T lymphocyte response in these mice, nor evidence of Iba1 immunoreactivity. Taken together, these results not only suggest a steep dose-response curve in terms of BU's ability to induce the appearance of GFP^+ cells in the first 4 weeks, but also that T lymphocytes and/or endothelial damage may be required for early population of the CNS by donor cells.

After this experiment we took a group of GFP chimeric mSOD mice to end-stage to look at the degree of cell entry with 60 mg/kg and 80 mg/kg after a period of 11 weeks. With both these groups, we saw much lower numbers in the mSOD mice than with either irradiation (Lewis *et al*., 2009) or 100 mg/kg BU.

There was a significant difference ($p < 0.05$) in the degree of entry between control and mSOD mice for both the 60 mg/kg and the 80 mg/kg groups, but the difference in the number of cells between these doses (46.2 ± 18.6 *vs.* 74.3 ± 44.5) was not significant.

A very limited increase in the number of cells in the control mice was also observed from the 4-week data. This further suggests that little additional cell entry or expansion occurs past the 3-4 week time point without neurodegeneration. It also supports Chinnery *et al*., who take the view that minimal cellular entry into the CNS parenchyma occurs under physiological conditions.

The largest notable difference between 4 week controls and age-matched end-stage controls was that there were more Iba^+ elongated cells at this later time point in both the 60 and 80 mg/kg BU (Figure 13), which may support the conclusions of Audoy-Remus *et al*., (2008) that undifferentiated rod-shaped cells are the precursors to elongated-morphology perivascular macrophages. It has been suggested that donor-derived monocytic cells may initially populate the spinal cord as perivascular macrophages and then move across the *glia limitans* into the CNS parenchyma, where they receive signals differentiate into stellate-shaped microglia (Guillemin & Brew, 2004). Although this cannot be confirmed by our work, one of the differences between control and mSOD mice treated with BU (besides the difference in total cell numbers) is the proportional increase in stellate-shaped cells that label with Iba1. Stellate GFP^+ cells were virtually non-

existent in our 60 and 80 mg/kg treated control mice, while in mSOD mice there was an average of 9.5 ± 8.6 of these cells in the 60 mg/kg mice, and 19.6 ± 17.4 in the 80 mg/kg. It has been suggested that CCL2 production, as a consequence of the neurodegeneration and microgliosis seen in ALS, may induce the entry of peripheral blood cells to the CNS (Appel *et al*., 2009). However, reports of diminished cell entry without tissue pre-conditioning (Ajami *et al*., 2007) suggest that endothelial cell activation may also be necessary for this to process to occur.

Lastly, additional CY treatment had quite a profound effect on the magnitude of cell entry seen with 80 mg/kg. The spinal cords of these mice appeared more akin to mSOD SJL/B6 mice treated with 100 mg/kg BU, rather than B6 mice treated with 80 mg/kg BU, as they displayed over 300 cells per section, many of which were $Iba1^+$ and of stellate and elongated morphology. Unlike BU, CY has poor CNS penetrance, and it is therefore improbable that is imparts any neuro-infammatory effect (Wiebe *et al*., 1992).

The number of T lymphocytes observed in the CNS of BU/CY treated mice was also unexpected. Between these animals, there was a mean of 42.7 $CD3^+$ cells per section, with 56.3% of them being of donor origin, but very few of these labelling for CD8. This low proportion of $CD8^+$ cells at disease end-stage might be explained however by reports that CY induces $CD4^+$ T cell polarization to a more anti-inflammatory phenotype, as well reduces the proportion of IFNγ-producing $CD8^+$ cells in the CNS (Karni *et al*., 2004).

5.3. Conclusions

Whole body irradiation has long been utilized as the main pre-conditioning method prior to allogeneic BMT, as it can provide robust engraftment of donor stem cells. However, previous attempts to use sub-myeloablative irradiation to induce the engraftment of autologous cells have had limited success (Huhn *et al*., 1999; Kang *et al*., 2001), possibly because of the steep dose-response curve associated with irradiation. Many of these studies have shown that under some conditions, transplanted haematopoietic cells are capable of taking up residence in the CNS and differentiating into parenchymal microglia. It has also been demonstrated that this phenomenon may be dependant on exposure of CNS tissue to gamma rays (Mildner *et al*., 2007). This exposure can induce widespread inflammation and cytokine production (Ramanan *et al*., 2010), disruption of BBB endothelial cells (Li *et al*., 2004), and increase the frequency of BM cell fusion with Purkinje neurons (Espejel *et al*., 2009). As these conditions are far from physiologically normal, I evaluated alternative pre-conditioning regimens for myeloablation.

BU represents an attractive pre-conditioning alternative for autologous bone marrow transplantation, as it is available as an intravenous formulation with reasonably predictable pharmacokinetics (Hsieh *et al*., 2007). I found BU doses as low as 60 mg/kg capable of producing transient myelosupression and stable chimerism in excess of 70% by 8 weeks post-transplant. I also found it easy to administer parentally in mice and well tolerated up to 100 mg/kg without

additional haematopoietic support. Additionally, unlike ionizing radiation, it does not ablate the adaptive immune compartment, which is critical in protecting the recipient from opportunistic infection.

However, a complication associated with doses greater than 80 mg/kg was the appearance of CD8+ T lymphocytes in the CNS, a phenomenon I attribute to drug-induced neuroinflammation. This finding is likely of clinical relevance if this protocol is ever to be used for the treatment of neurological disorders.

The work described in this thesis improves the potential for using haematopoietic cells as autologous treatment vehicles in neurodegenerative diseases by providing an alternative method for inducing BM-derived cells into the CNS. Additionally, these findings also increase the feasibility of generating stable mixed chimeric animals or near-complete reconstituted animals without the requirement for gamma irradiation.

References

Abbott NJ, Patabendige AA, Dolman DE, Yusof SR, Begley DJ. (2010) Structure and function of the blood-brain barrier. *Neurobiology of Disease*, 37:13-25.

Agrawal S, Anderson P, Durbeej M, van Rooijen N, Ivars F, Opdenakker G, Sorokin LM. (2006) Dystroglycan is selectively cleaved at the parenchymal basement membrane at sites of leukocyte extravasation in experimental autoimmune encephalomyelitis. *Journal of Experimental Medicine*, 203:1007-1019.

Ajami B, Bennett JL, Krieger C, Tetzlaff W, Rossi FM. (2007) Local self-renewal can sustain CNS microglia maintenance and function throughout adult life. *Nature Neuroscience,* 10(12):1538-1543.

Ajami B, Bennett JL, Krieger C, McNagny KM, Rossi FM. (2011) Infiltrating monocytes trigger EAE progression, but do not contribute to the resident microglia pool. *Nature Neuroscience,* 14(9):1142-1149.

Alexander GM, Erwin KL, Byers N, Deitch JS, Augelli BJ, Blankenhorn EP, Heiman-Patterson TD. (2004) Effect of transgene copy number on survival in the G93A SOD1 transgenic mouse model of ALS. *Molecular Brain Research,* 130(1-2):7-15.

Anam K, Black AT, Hale DA. (2006) Low dose busulfan facilitates chimerism and tolerance in a murine model. *Transplant Immunology,* 15:199–204.

Anderson PM. (2006) Amyotrophic lateral sclerosis associated with mutations in the CuZn superoxide dismutase gene. *Current Neurology Neuroscience Reports,* 6:37-46.

Andersson G, Illigens BM, Johnson KW, Calderhead D, LeGuern C, Benichou G, White-Scharf ME, Down JD. (2003) Nonmyeloablative conditioning is sufficient to allow engraftment of EGFP-expressing bone marrow and subsequent acceptance of EGFP-transgenic skin grafts in mice. *Blood*, 101(11):4305-4312.

Appel SH, Engelhardt JI, Henkel JS, Siklos L, Beers DR, Yen AA, Simpson EP, Luo Y, Carrum G, Heslop HE, Brenner MK, Popat U. (2008) Hematopoietic stem cell transplantation in patients with sporadic amyotrophic lateral sclerosis. *Neurology,* 71(17):1326-1334.

Appel SH, Beers DR, Henkel JS. (2009) T-cell microglial dialogue in Parkinson's Disease and amyotrophic lateral sclerosis: are we listening? *Trends in Immunology*, 31(1):7-17.

Audoy-Remus J, Richard JF, Soulet D, Zhou H, Kubes P, Vallieres L. (2008) Rod-shaped monocytes patrol the brain vasculature and give rise to perivascular macrophages under the influence of proinflammatory cytokines and angiopoietin-2. *The Journal of Neuroscience: The Official Journal of the Society for Neuroscience*, *28*(41):10187-10199.

Bacigalupo A, Vitale V, Corvò R, Barra S, Lamparelli T, Gualandi F, Mordini N, Berisso G, Bregante S, Raiola AM, Van Lint MT, Frassoni F. (2000) The combined effect of total body irradiation (TBI) and cyclosporin A (CyA) on the risk of relapse in patients with acute myeloid leukaemia undergoing allogeneic bone marrow transplantation. *British Journal of Haematology*, 108:99–104.

Banerjee R, Mosley RL, Reynolds AD, Dhar A, Jackson-Lewis V, Gordon PH, Przedborski S, Gendelman HE. (2008) Adaptive Immune Neuroprotection in G93A-SOD1 Amyotrophic Lateral Sclerosis Mice. *PLoS ONE*, 3(7):1-16.

Barker CF & Billingham RE (1977) Immunologically priviledged sites. *Advances in Immunology*, 25:1-54.

Barry C. (2003) Phenotypically Curing β-Thalassemic Mice in a Non-Myeloablative Setting, *Unpublished Honor's Thesis*, University of British Columbia, Vancouver, Canada.

Baron JL, Madri JA, Ruddle NH, Hashim G, Janeway CA. (1993) Surface expression of alpha 4 integrin by CD4 T cells is required for their entry into brain parenchyma. *Journal of Experimental Medicine*, 177:57-68.

Becher B, Bechmann I, Greter M. (2006) Antigen presentation in autoimmunity and CNS inflammation: how T lymphocytes recognize the brain. *Journal of Molecular Medicine*, 84:532-543.

Beelen DW, Quabeck K, Graeven U, Sayer HG, Mahmoud HK, Schaefer UW. (1989) Acute toxicity and first clinical results of intensive post-induction therapy using a modified busulfan and cyclophosphamide regimen with autologous bone marrow rescue in first remission of acute myeloid leukemia. *Blood*, 74:1507-1516.

Beers DR, Henkel JS, Xiao Q, Zhao W, Wang J, Yen AA, Siklos L, McKercher SR, Appel SH. (2006) Wild type microglia extend survival in PU.1 knockout mice with familial amyotrophic lateral sclerosis. *Proceedings of the National Academy of Sciences of the United States of America*, 103:16021-16026

Belka C, Budach W, Kortmann RD, Bamberg M (2001) Radiation induced CNS toxicity – molecular and cellular mechanisms *British Journal of Cancer*, 85(9):1233-1239.

Bishop JB & Wassom JS. (1986) Toxicological review of busulfan (Myleran). *Mutation Research*, 168:15–45.

Boeckh M, Nichols WG, Papanicolaou G, Rubin R, Wingard JR, Zaia Y. (2003) Cytomegalovirus in hematopoietic stem cell transplant recipients: Current status,

known challenges, and future strategies. *Biology of Blood and Marrow Transplantation*, 9(9):543-558.

Boillee S, Vande Velde C, & Cleveland DW. (2006a) ALS: A disease of motor neurons and their non-neuronal neighbors. *Neuron*, 52(1):39-59.

Boillee S, Yamanaka K, Lobsiger CS, Copeland NG, Jenkins NA, Kassiotis G, Kollias G, Cleveland DW. (2006b) Onset and progression in inherited ALS determined by motor neurons and microglia. *Science*, 312:1389-1392.

Bradley MB, Sattler MS, Raftopoulos H, Ward M, Grossman IR, Townes TM, Ryan TM, Bank A. (2002) Correction of phenotype in a Thalassemia mouse model using non-myeloablative marrow transplantation regimen. *Biology of Blood and Marrow Transplantation*, 8:453-461.

Buggia I, Locatelli F, Regazzi MB, and Zecca M. (1994) Busulfan. *Annals of Pharmacotherapy*, 28:1055–1062.

Calzascia T, Masson F, Di Berardino-Besson W, Contassot E, Wilmotte R, Aurrand-Lions M, Ruegg C, Dietrich PY, Walker PR. (2005) Homing phenotypes of tumour specific CD8 T cells are predetermined at the tumour site by cross-presenting APCs. *Immunity*, 22:175-184.

Cardona AE, Pioro EP, Sasse ME, Kostenko V, Cardona SM, Dijkstra IM, Huang D, Kidd G, Dombrowski S, Dutta R, Lee JC, Cook DN, Jung S, Lira SA, Littman DR, Ransohoff RM. (2006) Control of microglial neurotoxicity by the fractalkine receptor. *Nature Neuroscience*, 9:917-924.

Carman CV & Springer TA. (2004) A transmigratory cup in leukocyte diapedesis both through individual vascular endothelial cells and between them. *Journal of Cell Biology*,167:377–388.

Carman CV, Sage PT, Sciuto TE, de la Fuente MA, Geha RS, Ochs HD, Dvorak HF, Dvorak AM, Springer TA. (2007) Transcellular diapedesis is initiated by

invasive podosomes. *Immunity*, 26:784–797.

Chaney SG & Sancar A. (1996) DNA repair: enzymatic mechanisms and relevance to drug response. *Journal of the National Cancer Institute*, 88:1346-1360.

Chinnery HR, Ruitenberg MJ, McMenamin PG. (2010) Novel characterization of monocyte-derived cell populations in the meninges and choroid plexus and their rates of replenishment in bone marrow chimeric mice. *Journal of Neuropathology and Experimental Neurology*, *69*(9):896-909.

Chiu IM, Chen A, Zheng Y, Kosaras B, Tsiftsoglou SA, Vartanian TK, Brown RH, Carroll MC. (2008) T lymphocytes potentiate endogenous neuroprotective inflammation in a mouse model of ALS. *Proceedings of the National Academy of Sciences of the United States of America,* 105(46):17913-17918.

Choi C & Benveniste E. (2004) Fas ligand/Fas system in the brain: regulator of immune and apoptotic responses. *Brain Research Reviews*, 44:65-81.

Coisne C, Mao W, Engelhardt B. (2009) Cutting edge: Natalizumab blocks adhesion but not initial contact of human T cells to the blood-brain barrier in vivo in an animal model of multiple sclerosis. *Journal of Immunology*, 182:5909-5913.

DeJesus-Hernandez M, Mackenzie IR, Boeve BF, Boxer AL, Baker M, Rutherford NJ, Nicholson AM, Finch NA, Flynn H, Adamson J, Kouri N, Wojtas A, Sengdy P, Hsiung GY, Karydas A, Seeley WW, Josephs KA, Coppola G, Geschwind DH, Wszolek ZK, Feldman H, Knopman DS, Petersen RC, Miller BL, Dickson DW, Boylan KB, Graff-Radford NR, Rademakers R. (2011) Expanded GGGGCC hexanucleotide repeat in non-coding region of C9ORF72 causes chromosome 9p-linked fronto-temporal dementia and amyotrophic lateral sclerosis. *Neuron*, 72(2):245-256.

Del Maschio A, De Luigi A, Martin-Padura I, Brockhaus M, Bartfai T, Fruscella P,

Adorini L, Martino G, Furlan R, De Simoni MG, Dejana E. (1999) Leukocyte recruitment in the cerebrospinal fluid of mice with experimental meningitis is inhibited by an antibody to junctional adhesion molecule (JAM). *Journal of Experimental Medicine*, 190:1351-1356.

Di Giorgio FP, Carrasco MA, Siao MC, Maniatis T, Eggan K. (2007) Non–cell autonomous effect of glia on motor neurons in an embryonic stem cell–based ALS model. *Nature Neuroscience*, 10:608-614.

Djukic M Mildner A, Schmidt H, Czesnik D, Brück W, Priller J, Nau R, Prinz M. (2006) Circulating monocytes engraft in the brain, differentiate into microglia and contribute to the pathology following meningitis is mice. *Brain*, 129: 2394-2403.

Dore-Duffy P. (2008) Pericytes: pluripotent cells of the blood brain barrier. *Current Pharmaceutical Design*, 14:1581-1593

Dunn CDR. (1974) The chemical and biological properties of busulphan ("myleran"). *Experimental Haematology*, 2:101-117.

Engelhardt J, Tajti J, Appel SH. (1993) Lymphocytic infiltrates in the spinal cord in amyotrophic lateral sclerosis. *Archives of Neurology*, 50:30-36.

Engelhardt B. (2008) The blood-central nervous system barriers actively control immune cell entry into the central nervous system. *Current Pharmaceutical Design*, 14:1555-1565.

Engelhardt B & Coisne C. (2011) Fluids and barriers of the CNS establish immune privilege by confining immune surveillance to a two-walled castle moat surrounding the CNS castle. *Fluids and Barriers of the CNS*, 8:4.

Espejel S, Romero R, Alvarez-Buylla A. (2009). Radiation damage increases purkinje neuron heterokaryons in neonatal cerebellum. *Annals of Neurology*, *66*(1):100-109.

Ferrara JL, Levine JE, Reddy P, Holler E. (2009) Graft-versus-host disease. *Lancet*, 373:1550-1561.

Fischer-Lindahl K. (1997) On naming MHC haplotypes: functional significance of MHC class Ib alleles. *Immunogenetics,* 46:53-62.

Fitzsimmons WE, Ghalie R, Kaizer H. (1990) The effect of hepatic enzyme inducers on busulfan neurotoxicity and myelotoxicity. *Cancer Chemotherapy and Pharmacology*, 127:226-228.

Galea I, Bechmann I, Perry VH. (2007) What is immune privilege (not)? *Trends in Immunology*, 28:12-18.

Gibbs Jp, Murray G, Risler L, Chien JY, Dev R, Slatery JT. (1997) Age-dependent tetrahydrothiophenium ion formation in young children and adults receiving high-dose busulfan. *Cancer Research*, 57:5509-5516.

Ginhoux F, Greter M, Leboeuf M, Nandi S, See P, Gokhan S, Mehler MF, Conway SJ, Ng LG, Stanley RE, Samokhvalov IM, Merad M. (2010) Fate mapping analysis reveals that adult microglia derive from primitive macrophages. *Science*, 330(6005):841-845.

Göbel K, Melzer N, Herrmann AM, Schuhmann MK, Bittner S, Ip CW, Hünig T, Meuth SG, Wiendl H. (2010) Collateral neuronal apoptosis in CNS gray matter during an oligodendrocyte-directed $CD8^+$ T cell attack. *Glia*, 58(4):469-480.

Gonzalez-Scarano F & Baltuch G. (1999) Microglia as mediators of inflammatory and degenerative diseases. *Annual Review of Neuroscience*, 22:219-240.

Gowing G, Lalancette-Herbert M, Audet JN, Dequen F, Julien JP. (2009) Macrophage colony stimulating factor (M-CSF) exacerbates ALS disease in a mouse model through altered responses of microglia expressing mutant superoxide dismutase. *Experimental Neurology*, 220:267-275.

Graesser D, Solowiej A, Bruckner M, Osterweil E, Juedes A, Davis S, Ruddle N, Engelhardt B, Madri JM. (2002) Changes in vascular permeability and early onset of experimental autoimmune encephalomyelitis in PECAM-1(CD31) deficient mice. *Journal of Clinical Investigation*, 109:383-392.

Grochow LB, Jones RJ, Brundrett RB, Braine HG, Chen TL, Saral R, Santos GW, Colvin OM. (1989) Pharmacokinetics of busulfan: correlation with veno-occlusive disease in patients undergoing bone marrow transplantation. *Cancer Chemotherapy and Pharmacology*, 25:55-61.

Gurney ME, Pu H, Chiu AY, Dal Canto MC, Polchow CY, Alexander DD, Caliendo J, Hentati A, Kwon YW, Deng HX, Chen W, Zhai P, Sufit RL, Siddique T. (1994) Motor neuron degeneration in mice that express a human cu,zn superoxide dismutase mutation. *Science*, 264(5166):1772-1775.

Haorah J, Heilman D, Knipe B, Chrastil J, Leibhart J, Ghorpade A, Miller DW, Persidsky Y. (2005) Ethanol-induced activation of myosin light chain kinase leads to dysfunction of tight junctions and blood-brain barrier compromise. *Alcoholism: Clinical and Experimental Research*, 29:999-1009.

Hassan M & Ehrsson H. (1987) Metabolism of 14C-busulfan in isolated perfused rat liver. *European Journal of Drug Metabolism and Pharmacokinetics*, 12:71-76.

Hassan M, Oberg G, Ehrsson H, Ehrnebo M, Wallin I, Smedmyr B, Tötterman T, Eksborg S, Simonsson B. (1989a) Pharmacokinetic and metabolic studies of high-dose busulphan in adults. *European Journal of Clinical Pharmacology*, 36:525-530.

Hassan M, Erhsson H, Smedmyr B, Totterman T, Wallin I, Oberg G, Simonsson B. (1989b) Cerebrospinal fluid and plasma concentrations of busulfan during high-dose therapy. *Bone Marrow Transplantation*, 4:113-114.

Hassan M, Oberg G, Ericson K, Ehrsson H, Eriksson L, Ingvar M, Stone-Elander S, Thorell JO, Smedmyr B, Warne N, Widen L.(1992) In vivo distribution of [11C]-busulfan in cynomolgus monkey and in the brain of a human patient. *Cancer Chemotherapy and Pharmacology*, 30(2):81–85.

Hassan M, Ehrsson H, Ljungman P. (1996) Aspects concerning busulfan pharmacokinetics and bioavailability. *Leukemia & Lymphoma*, 22(5-6):395-407.

Hassan M. (1999) The role of busulfan in bone marrow transplantation. *Medical Oncology*, 16:166-176.

Hassan M, Ljungman P, Ringden O, Hassan Z, Oberg G, Nilsson C, Bekassy A, Bielenstein M, Abdel-Rehim M, Georen S, Astner L. (2000) The effect of busulphan on the pharmacokinetics of cyclophosphamide and its 4-hydroxy metabolite: time interval influence on therapeutic efficacy and therapy-related toxicity. *Bone Marrow Transplantation*. 25:915–924

Henkel JS, Beers DR, Siklos L, Appel SH. (2006) The chemokine MCP-1 and the dendritic and myeloid cells it attracts are increased in the mSOD1 mouse model of ALS. *Molecular and Cellular Neuroscience*, 31:427-437.

Gowing G & Svendsen CN. (2011) Stem cell transplantation for motor neuron disease: Current approaches and future perspectives. *Neurotherapeutics*, 8:591-606.

Holmoy T. (2008) T cells in amyotrophic lateral sclerosis. *European Journal of Neurology*, 15:360-366.

Hsieh MM, Langemeijer S, Wynter A, Phang OA, Kang EM, Tisdale JF. (2007) Low-dose parenteral busulfan provides an extended window for the infusion of hematopoietic stem cells in murine hosts. *Experimental* Hematology, 35(9):1415-1420.

Huang D, Shi F-D, Jung S, Pien GC, Wang J, Salazar-Mather TP, He TT, Weaver JT, Ljunggren HG, Biron CA, Littman DR, Ransohoff RM. (2006) The neuronal chemokine CX3CL1/fractalkine selectively recruits NK cells that modify experimental autoimmune encephalomyelitis within the central nervous system. *FASEB Journal*, 20:896-905.

Huber JD, Egleton RD and Davis TP. (2001) Molecular physiology and pathophysiology of tight junctions in the blood-brain barrier. *Trends in Neurosciences*, 24:719-725.

Huhn RD, Tisdale JF, Agricola B, Metzger ME, Donahue RE, Dunbar CE. (1999) Retroviral marking and transplantation of rhesus hematopoietic cells by nonmyeloablative conditioning. *Human Gene Therapy*, 10:1783-1790.

Ivey NS, MacLean AG, Lackner AA. (2009) AIDS and the blood-brain barrier. *Journal of Neurovirology*, 15(2):111-122.

Iwamoto T, Hiraku Y, Oikawa S, Mizutani H, Kojima M, Kawanishi S. (2004) DNA intra-strand cross-link at the 5′-GA-3′ sequence formed by busulfan and its role in the cytotoxic effect. *Cancer Science*, 95:454-458.

Jaarsma D, Haasdijk ED, Grashorn JA, Hawkins R, van Duijn W, Verspaget HW, London J, Holstege JC. (2000) Human Cu/Zn superoxide dismutase (SOD1) overexpression in mice causes mitochondrial vacuolization, axonal degeneration, and premature motor neuron death and accelerates motoneuron disease in mice expressing a familial amyotrophic lateral sclerosis mutant SOD1. *Neurobiology of Disease*, 7:623-643.

Jaarsma D, Teuling E, Haasdijk ED, De Zeeuw CI, Hoogenraad CC. (2008) Neuron-specific expression of mutant superoxide dismutase is sufficient to induce amyotrophic lateral sclerosis in transgenic mice. *The Journal of Neuroscience: The Official Journal of the Society for Neuroscience*, 28(9):2075-2088.

Johnson AK & Gross PM. (1993) Sensory circumventricular organs and brain homeostatic pathways. *FASEB J*, 7:678-686.

Jopling C & Rosendaal M. (2001) A cautionary tale: how to delete mouse haemopoietic stem cells with busulphan. *British Journal of Haematology*, 113:970-974.

Kalifa C, Hartmann O, Demeocq F, Vassal G, Couanet D, Terrier-Lacombe MJ, Valteau D, Brugieres L, Lemerle J. (1992) High-dose busulfan and thiotepa with autologous bone marrow transplantation in childhood malignant brain tumors: a phase II study. *Bone Marrow Transplantation*, 4:227-233.

Kang EM, Hanazano Y, Frare P, Vanin EF, De Witte M, Metzger M, Liu JM, Tisdale JF. (2001) Persistent low-level engraftment of rhesus peripheral blood progenitor cells transduced with the fanconi anemia C gene after conditioning with low-dose irradiation. *Molecular Therapy*, 3:911-919.

Karni A, Abraham M, Monsonego A, Cai G, Freeman GJ, Hafler D, Khoury SJ, Weiner HL. (2004) Cyclophosphamide modulates $CD4^+$ T cells into a T helper type 2 phenotype and reverses increased IFN-? production of $CD8^+$ T cells in secondary progressive multiple sclerosis. *Journal of Neuroimmunology*, 146:189-198.

Kawamata T, Akiyama H, Yamada T, McGeer PL. (1992) Immunologic reactions in amyotrophic lateral sclerosis brain and spinal cord tissue. *American Journal of Pathology*, 140:691-707.

Keep RF & Jones HC. (1990) A morphometric study on the development of the lateral ventricle choroid plexus, choroid plexus capillaries and ventricular ependyma in the rat. *Developmental Brain Research*, 56:47– 53.

Kerfoot SM, Norman MU, Lapointe BM, Bonder CS, Zbytnuik L, Kubes P. (2006) Reevaluation of P-selectin and alpha 4 integrin as targets for the treatment of

experimental autoimmune encephalomyelitis. *Journal of Immunology,* 176:6225-6234.

Krueger M & Bechmann I. (2010) CNS pericytes: concepts, misconceptions, and a way out. *Glia*, 58:1–10.

Lewis CA, Solomon JN, Rossi FM, Krieger C. (2009) Bone marrow-derived cells in the central nervous system of a mouse model of amyotrophic lateral sclerosis are associated with blood vessels and express CX(3)CR1. *Glia,* 57(13):1410-1419.

Lewis CA, Manning J, Rossi F, Krieger C. (2012) The Neuroinflammatory Response in ALS: The Roles of Microglia and T Cells. *Neurology Research International*, 2012:803701.

Li YQ, Chen P, Jain V, Reilly RM, Wong CS. (2004) Early radiation-induced endothelial cell loss and blood-spinal cord barrier breakdown in the rat spinal cord. *Radiation Research*, 161(2):143-152.

Litzow MR, Pérez WS, Klein JP, Bolwell BJ, Camitta B, Copelan EA, Gale RP, Giralt SA, Keating A, Lazarus HM, Marks DI, McCarthy PL, Miller CB, Milone G, Prentice HG, Russell JA, Schultz KR, Trigg ME, Weisdorf DJ, Horowitz MM. (2002) Comparison of outcome following allogeneic bone marrow transplantation with cyclophosphamide: total body irradiation versus busulphan-cyclophosphamide conditioning regimens for acute myelogenous leukaemia in first remission. *British Journal of Haematology*, 119: 1115–1124.

Liu Y, Teige I, Birnir B, Issazadeh-Navikas S. (2006) Neuron-mediated generation of regulatory T cells from encephalitogenic T cells suppresses EAE. *Nature Medicine*, 12:518–525.

Locksley R. (2009) Nine lives: Plasticity among helper cell subsets. *Journal of Experimental Medicine*, 206:1643-1646.

Löscher W & Potschka H. (2005) Role of drug efflux transporters in the brain for drug disposition and treatment of brain diseases. *Progress in Neurobiology*, 76:22–76.

Malm T, Koistinaho M, Muona A, Magga J, Koistinaho J. (2010) The role and therapeutic potential of monocytic cells in alzheimer's disease. *Glia*, 58(8):889-900.

Marchand DH. (1987) The role of glutathione and glutathione s-transferases in the metabolism of busulfan. *Unpublished Master's Thesis*, University of Minnesota, Twin Cities, USA.

Mauch P, Down JD, Warhol M, Hellman S. (1988) Recipient preparation for bone marrow transplantation. I. Efficacy of total-body irradiation and busulfan. *Transplantation*, 46:205-210.

Medawar PB. (1948) Immunity to homologous grafted skin. III. The fate of skin homografts transplanted to the brain, to subcutaneous tissue and to anterior chamber of the eye. *British Journal of Experimental Pathology,* 29:58-69.

Melzer N, Meuth SG, Wiendl H. (2009) $CD8^+$ T cells and neuronal damage: direct and collateral mechanisms of cytotoxicity and impaired electrical excitability. *FASEB Journal*, 23**:**3659-3673.

Mildner A, Schmidt H, Nitsche M, Merkler D, Hanisch UK, Mack M, Heikenwalder M, Bruck W, Priller J, Prinz M. (2007) Microglia in the adult brain arise from ly-6ChiCCR2$^+$ monocytes only under defined host conditions. *Nature Neuroscience*, *10*(12):1544-1553.

Moisse K, & Strong M, (2006) Innate immunity in amyotrophic lateral sclerosis. *Biochimica et Biophysica Acta*, 1762:1083-1093.

Mott RT, Ait-Ghezala G, Town T, Mori T, Vendrame M, Zeng J, Ehrhart J, Mullan M, Tan J. (2004) Neuronal expression of CD22: novel mechanism for inhibiting

microglial proinflammatory cytokine production. *Glia*, 46**:**369-379.

Mrass P, Takano H, Ng LG, Daxini S, Lasaro MO, Iparraguirre A, Cavanagh LL, von Andrian UH, Ertl HC, Haydon PG, Weninger W. (2006) Random migration precedes stable target cell interactions of tumor infiltrating T cells. *Journal of Experimental Medicine*, 203:2749-2761.

Muller-Sieburg C, Cho R, Thoman M, Adkins B, Sieburg H. (2002) Deterministic regulation of hematopoietic stem cell self-renewal and differentiation. *Blood*, 100: 1302-1309.

Napoli I & Neumann H. (2009) Microglial clearance function in health and disease. *Neuroscience*, 158(3)**:**1030-1038.

Neumann H, Medana IM, Bauer J, Lassmann H. (2002) Cytotoxic T lymphocytes in autoimmune and degenerative CNS diseases. *Trends in Neurosciences*, *25*(6):313-319.

Nevozhay D & Opolski A (2006) Key factors in experimental mouse hematopoietic stem cell transplantation. *Archivum Immunologiae Et Therapiae Experimentalis*, *54*(4):253-269.

Nitsch R*,* Pohl EE*,* Smorodchenko A*,* Infante-Duarte C*,* Aktas O*,* Zipp F. (2004) Direct impact of T cells on neurons revealed by two-photon microscopy in living brain tissue. *Journal of Neuroscience*, 24**:**2458–2464.

Nottet HS, Persidsky Y, Sasseville VG, Nukuna AN, Bock P, Zhai QH, Sharer LR, McComb RD, Swindells S, Soderland C, Gendelman HE. (1996) Mechanisms for the trans-endothelial migration of HIV-1-infected monocytes into brain. *Journal of* Immunology, 156:1284–1295.

Padovani-Claudio DA, Liu L, Ransohoff RM, Miller RH. (2006) Alterations in the oligodendrocyte lineage, myelin, and white matter in adult mice lacking the chemokine receptor CXCR2. *Glia*, 54:471-483.

Pardridge WM. (2007) Blood-brain barrier delivery. *Drug Discovery Today*, 12:54-61.

Philips T & Robberecht W. (2011) Neuroinflammation in amyotrophic lateral sclerosis: Role of glial activation in motor neuron disease. *Lancet Neurology*, 10(3):253-263.

Piccio L, Rossi B, Scarpini E, Laudanna C, Giagulli C, Issekutz AC, Vestweber D, Butcher EC, Constantin G. (2002) Molecular mechanisms involved in lymphocyte recruitment in inflamed brain microvessels: critical roles for P-selectin glycoprotein ligand-1 and heterotrimeric G(i)-linkedreceptors. *Journal of Immunology*, 168:1940-1949.

Priller J, Prinz M, Heikenwalder M, Zeller N, Schwarz P, Heppner FL, Aguzzi A. (2006) Early and rapid engraftment of bone-marrow derived microglia in scrapie. *Journal of Neuroscience*, 26:11753-11762.

Prinz M, Priller J, Sisodia SS, Ransohoff RM. (2011) Heterogeneity of CNS myeloid cells and their roles in neurodegeneration. *Nature Neuroscience*, 14(10):1-9.

Ransohoff RM, Kivisakk P, Kidd G. (2003) Three or more routes for leukocyte migration into the central nervous system. *Nature Reviews Immunology*, 3:569-581

Ransohoff RM. (2009) Chemokines and chemokine receptors: standing at the crossroads of immunobiology and neurobiology. *Immunity*, 31:711-721.

Ransohoff R & Cardona A. (2010) The myeloid cells of the central nervous system parenchyma. *Nature*, 468:253-26.

Ramanan S, Zhao W, Riddle DR, Robbins ME. (2010) Role of PPARs in radiation-induced brain injury. *Peroxisome Proliferator-Activated Receptors Research,* 2010:234975.

Reaume AG, Elliot JL, Hoffman EK, Kowall NW, Ferrante RJ, Siwek DF, Wilcox HM, Flood DG, Beal MF, Brown RH, Scott RW, Snider WD. (1996) Motor neurons in Cu/Zn superoxide dismutase-deficient mice develop normally but exhibit enhanced cell death after axonal injury. *Nature Genetics*, 13(1):43-47.

Renton AE, Majounie E, Waite A, Simón-Sánchez J, Rollinson S, Gibbs JR, Schymick JC, Laaksovirta H, van Swieten JC, Myllykangas L, Kalimo H, Paetau A, Abramzon Y, Remes AM, Kaganovich A, Scholz SW, Duckworth J, Ding J, Harmer DW, Hernandez DG, Johnson JO, Mok K, Ryten M, Trabzuni D, Guerreiro RJ, Orrell RW, Neal J, Murray A, Pearson J, Jansen IE, Sondervan D, Seelaar H, Blake D, Young K, Halliwell N, Callister JB, Toulson G, Richardson A, Gerhard A, Snowden J, Mann D, Neary D, Nalls MA, Peuralinna T, Jansson L, Isoviita VM, Kaivorinne AL, Hölttä-Vuori M, Ikonen E, Sulkava R, Benatar M, Wuu J, Chiò A, Restagno G, Borghero G, Sabatelli M, Heckerman D, Rogaeva E, Zinman L, Rothstein JD, Sendtner M, Drepper C, Eichler EE, Alkan C, Abdullaev Z, Pack SD, Dutra A, Pak E, Hardy J, Singleton A, Williams NM, Heutink P, Pickering-Brown S, Morris HR, Tienari PJ, Traynor BJ. (2011) A hexanucleotide repeat expansion in C9ORF72 is the cause of chromosome 9p21-linked ALS-FTD. *Neuron*, 72(2):257-268.

Sadeghi B, Aghdami N, Hassan Z, Forouzanfar M, Rozell B, Abedi-Valugerdi M, Hassan M. (2008) GVHD after chemotherapy conditioning in allogeneic transplanted mice. *Bone Marrow Transplantation*, 42:807-818.

Sallusto F, Geginat J, Lanzavecchia A. (2004) Central memory and effector memory T cell subsets: function, generation, and maintenance. *Annual Review of Immunology*, 22:745–763.

Seder R & Ahmed R, (2003) Similarities and differences is $CD4^+$ and $CD8^+$ effector and memory T cell generation. *Nature Immunology*, 4:835-842.

Siffrin V, Radbruch H, Glumm R, Niesner R, Paterka M, Herz J, Leuenberger T, Lehmann SM, Luenstedt S, Rinnenthal JL, Laube G, Luche H, Lehnardt S, Fehling H Griesbeck O, and Zipp F. (2010) In Vivo Imaging of Partially Reversible Th17 Cell-Induced Neuronal Dysfunction in the Course of Encephalomyelitis. *Immunity*, 33:424-436.

Simard AR & Rivest S. (2004) Bone marrow stem cells have the ability to populate the entire central nervous system into fully differentiated parenchymal microglia. *FASEB Journal*, 18(9):998-1000.

Snell GD, Hoecker G, Amos DB, and Stimpfling JH. (1964) A revised nomenclature for the histocompatibility-2 locus of the mouse. *Transplantation*, 2: 777–784.

Snell RG, MacMillan JC, Cheadle JP, Fenton I, Lazarou LP, Davies P, MacDonald ME, Gusella JF, Harper PS, Shaw DJ. (1993) Relationship between trinucleotide repeat expansion and phenotypic variation in Huntington's disease. *Nature Genetics*, 4(4):393-397.

Sobel RA, Mitchell ME, Fondren G. (1990) Intercellular Adhesion Molecule-1 (ICAM-1) in cellular immune reactions in the human central nervous system. *American Journal of Pathology,* 136:1309-1316.

Solomon JN, Lewis CA, Ajami B, Corbel SY, Rossi FM, Krieger C. (2006) Origin and distribution of bone marrow-derived cells in the central nervous system in a mouse model of amyotrophic lateral sclerosis. *Glia, 53*(7):744-753.

Sospedra M & Martin R. (2005) Immunology of multiple sclerosis. *Annual Review of Immunology*, 23:683-747.

Steiner O, Coisne C, Cecchelli R, Boscacci R, Deutsch U, Engelhardt B, Lyck R. (2010) Differential roles for endothelial ICAM-1, ICAM-2, and VCAM-1 in shear-resistant T cell arrest, polarization, and directed crawling on blood-brain barrier

endothelium. *Journal of Immunology*, 185:4846-4855.

Stotler C, Bolwell B, Sobecks R, Dean R, Serafino S, Rybicki L, Andresen S, Pohlman B, Kalaycio M, and Copelan E. (2010) Are backup BM harvests worthwhile in unrelated donor allogeneic transplants? *Bone Marrow Transplantation*, 45:49-52.

Strazielle N & Ghersi-Egea JF. (2013) Physiology of Blood-Brain Interfaces in Relation to Brain Disposition of Small Compounds and Macromolecules. *Molecular Pharmaceutics*, In Press.

Szilvassy SJ, Bass MJ, Van Zant G, Grimes B. (1999) Organ-selective homing defines engraftment kinetics of murine hematopoietic stem cells and is compromised by ex vivo expansion. *Blood*, *93*(5):1557-1566.

Takeshita Y & Ransohoff RM. (2012), Inflammatory cell trafficking across the blood–brain barrier: chemokine regulation and *in vitro* models. *Immunological Reviews*, 248:228–239.

Troost D, Troost D, Van den Oord JJ, Vianney de Jong JM. (1990) Immunohistochemical characterization of the inflammatory infiltrate in amyotrophic lateral sclerosis. *Neuropathology and Applied Neurobiology*, 16:401-410.

Trajkovic V, Vuckovic O, Stosic-Grujicic S, Miljkovic D, Popadic D, Markovic M, Bumbasirevic *V*, Backovic A, Cvetkovic I, Harhaji L, Ramic Z, Mostarica Stojkovic M. (2004) Astrocyte-induced regulatory T cells mitigate CNS autoimmunity. *Glia*, 47:168–179.

Turner MR, Cagnin A, Turkheimer FE, Miller CC, Shaw CE, Brooks DJ, Leigh PN, Banati RB. (2004) Evidence of widespread cerebral microglial activation in amyotrophic lateral sclerosis: an [11C](R)-PK11195 positron emission tomography study. *Neurobiology of Disease*, 15:601–609.

Turner BJ & Talbot K. (2008) Transgenics, toxicity and therapeutics in rodent models of mutant SOD1-mediated familial ALS. *Progress in Neurobiology*, 85:94-134.

Ushiki T, Kizaka-Kondoh S, Ashihara E, Tanaka S, Masuko M Hirai H, Kimura *S*, Aizawa Y, Maekawa *T*, Hiraoka M. (2010) Noninvasive Tracking of Donor Cell Homing by Near-Infrared Fluorescence Imagining Shortly after Bone Marrow Transplantation. *PLoS ONE*, 5(6):1-12.

Vajkoczy P, Laschinger M, Engelhardt B. (2001) Alpha4-integrin-VCAM-1 binding mediates G protein-independent capture of encephalitogenic T cell blasts to CNS white matter microvessels. *Journal of Clinical Investigation*, 108:557-565.

Vallieres L & Sawchenko PE. (2003) Bone marrow-derived cells that populate the adult mouse brain preserve their hematopoietic identity. *Journal of Neuroscience*, 23:5:197-207.

Vassal G, Hartmann O, Benhamou E. (1990) Busulfan and veno-occlusive disease of the liver. *Annals of Internal Medicine*, 112:881.

Wiebe VJ, Smith BR, DeGregorio MW, Rappeport JM. (1992) Pharmacology of agents used in bone marrow transplant conditioning regimens. *Critical Reviews in Oncology/Hematology*, 13:241–270.

Winkler EA, Bell RD, Zlokovic BV. (2011) Central nervous system pericytes in health and disease. *Nature* Neuroscience,14:1398–1405.

Wu C, Ivars F, Anderson P, Hallmann R, Vestweber D, Nilsson P, Robenek H, Tryggvason K, Song J, Korpos E, Loser K, Beissert S, Georges-Labouesse E, Sorokin LM. (2009) Endothelial basement membrane laminin alpha5 selectively inhibits T lymphocyte extravasation into the brain. *Nature Medicine*,15:519-527.

Yeager AM, Shinn C, Shinohara M, Pardoll DM. (1993) Hematopoietic stem cell transplantation in the twitcher mouse. The effects of pretransplant conditioning with graded doses of busulfan. *Transplantation,* 56(1):185-190.

Zeng L, Jia L, Xu S, Yan Z, Ding S, Xu K, Wang L. (2010) Vascular endothelium changes after conditioning in hematopoietic stem cell transplantation: role of cyclophosphamide and busulfan. *Transplant Proceedings*, 42:2720–2724.

Appendix 1: Protocols.

G93A Mutant SOD Genotyping

Reagents:

Proteinase K

Ribonuclease A

Chelex 100

Deoxyribonucleotide triphosphates (dNTPs)

Primers (Invitrogen) :

Sense (mSOD1): CAT CAG CCC TAA TCC ATC TGA

Antisense (mSOD2) : CGC GAC TAA CAA TCA AAG TGA

Solutions:

TE, pH 8.0: 10 mM TrisCl: 60.55 mg, 1 mM EDTA: 16.81 mg, Top up to 50 mL with ddH20

Low TE, pH 7.6: 10x dilution of TE with ddH20

Proteinase K: 20 mg/mL in ddH20

RNase A: 10 mg/ml in ddH20

Chelex: 5% w/v in low TE

dNTPs (2 mM): 10 µL of dCTP, dTTP, dGTP, dATP in 460 µL ddH20

Protocol:

1. Collect ear punch tissue (store at -20 deg C)
2. Create DNA extraction buffer (per 2 samples)
    a) Chelex – 250 µL
    b) Proteinase K – 25 µL
    c) RNase A – 25 µL
3. Add 150 µL buffer to each sample and place in 55 deg C bath for 30 min, vortex after 15 min
4. Place in 100 deg C bath for 10 min
5. Centrifuge at 12000 rpm for 5 min
6. Extract 1 µL supernatant from each sample for DNA template (store at -20 deg C)
7. Create PCR reaction bugger (for each sample)
    a) Primer 1 – 0.5 µL
    b) Primer 2 – 0.5 µL

c) 10x buffer – 2.5 µL

d) dNTPs – 2.5 µL

e) MgCl2 – 0.5 µL

f) ddH20 – 17.2 µL

g) Taq – 0.3 µL

8. Run PCR cycle
9. Run on 1% agarose gel in 1x TBE running buffer
10. Add 1-2 µL bromophenol blue to PCR product and load 10 µL of PCR product plus dye each column in the gel
11. Run at 100V for approx. 30 min
12. 132 bp band indicates presence of mSOD transgene

Bone Marrow Transplantation

Solutions:

ACK lysis buffer (Invitrogen)

FACS buffer:

1x PBS – 500 mL

2% FBS – 10 mL

2 mM EDTA – 0.1489 g

Procedure:

1. Euthanize GFP donor with CO2
2. Cut skin at abdomen, pull down to expose legs
3. Cut legs from body and remove surrounding muscular tissue from femur and tibiae
4. Place bones in dish of 1x PBS
5. Cut bones at each end to expose marrow cavity
6. Flush marrow from cavity into petri dish using syringe loaded with FACS buffer and fitted with 25 ¾ guage needle
7. Break up clumped marrow by agitating solution with the syringe (sans needle)
8. Transfer BM solution to Falcon tube and centrifuge at 1500 rpm for 5 minutes
9. Remove supernatant and re-suspend in 1 mL RBC lysis buffer on ice for 9-10 minutes
10. Top up Falcon tube with FACS buffer to quench reaction and centrifuge at 1500 rpm for 5 minutes
11. Remove supernatant and re-suspend in 1 mL PBS
12. Pass solution through 40 µm filter
13. Count cells using Reichert haemocytometer
    a) add 10 µL of cell solution to 1 mL FACS buffer
    b) add 10 µL of diluted cells to haemocytometer chamber
    c) count cells in four grids surrounding central grid
    d) cells/mL: sum of grids/4 x 100 x 10000
14. Dilute solution with PBS to appox 1,500,000 cells per 400 µL
15. Inject desired number of cells into recipient mouse *via* tail vein
16. Collect weekly blood to assess reconstitution *via* flow cytometry